Synchrotron Radiation & Chemistry: Redox Reactions and Energy

Dipartimento di Fisica e Chimica
Università di Palermo

Antonino Martorana
XIV School of Synchrotron Radiation
Muggia, 18-29 September 2017

Case studies

- **batteries**
- CO_2 capture by Chemical-Looping Combustion (CLC)
- electrode-electrolyte interdiffusion processes
- *operando* investigation of Fuel Cell

CHEMISTRY OF MATERIALS

Article

pubs.acs.org/cm

Comprehensive Investigation of the $Na_3V_2(PO_4)_2F_3$–$NaV_2(PO_4)_2F_3$ System by Operando High Resolution Synchrotron X-ray Diffraction

M. Bianchini,[†,‡,§,⊥] F. Fauth,[∥] N. Brisset,[‡] F. Weill,[‡] E. Suard,[§] C. Masquelier,[†,⊥,#] and L. Croguennec*[,‡,⊥,#]

[†]Laboratoire de Réactivité et de Chimie des Solides, CNRS-UMR#7314, Université de Picardie Jules Verne, F-80039 Amiens Cedex 1, France

[‡]CNRS, Univ. Bordeaux, Bordeaux INP, ICMCB UPR 9048, F-33600 Pessac, France

[§]Institut Laue-Langevin, 71 Avenue des Martyrs, F-38000 Grenoble, France

[∥]CELLS - ALBA synchrotron, E-08290 Cerdanyola del Vallès, Barcelona, Spain

[⊥]RS2E, Réseau Français sur le Stockage Electrochimique de l'Energie, FR CNRS 3459, F-80039 Amiens Cedex, France

[#]ALISTORE-ERI European Research Institute, FR CNRS 3104, F-80039 Amiens Cedex, France

Supporting Information

ABSTRACT: $Na_3V_2(PO_4)_2F_3$ is a positive electrode material for Na-ion batteries which is attracting strong interest due to its high capacity, rate capability, and long-term cycling stability. The sodium extraction mechanism from this material has been always described in the literature as a straightforward solid solution, but several hints point toward a more complicated phase diagram. In this work we performed high angular resolution synchrotron radiation diffraction measurements, realized operando on sodium batteries upon charge. We reveal an extremely interesting phase diagram, created by the successive crystallization of four intermediate phases before the end composition $NaV_2(PO_4)_2F_3$ is reached. Only one of these phases undergoes a solid solution reaction, in the interval between 1.8 and 1.3 Na per formula unit. The ability to resolve weak Bragg reflections allowed us to reveal differences in terms of symmetry among the phases, to determine their previously unknown space groups, and to correlate them with sodium (dis)ordering in the structure. Rietveld refinements enabled us to follow fine structural modifications in great detail. Intermediate identified phases are not simply described by their unit cell parameters, but bond-length variations can be tracked, as well as polyhedral distortions and site occupancy factors for mobile sodium ions. For $NaV_2(PO_4)_2F_3$ a full crystal structure determination was also carried out for the first time directly from operando measurements, assigning it to the $Cmc2_1$ space group and revealing two vanadium environments: V^{3+} and V^{5+}. Our study demonstrates that improved angular resolution and high intensity diffraction data are key parameters for direct observation of fine reaction pathways in electrode materials and that the obtained insight is crucial for the understanding of (de)intercalation mechanisms in Na-ion batteries.

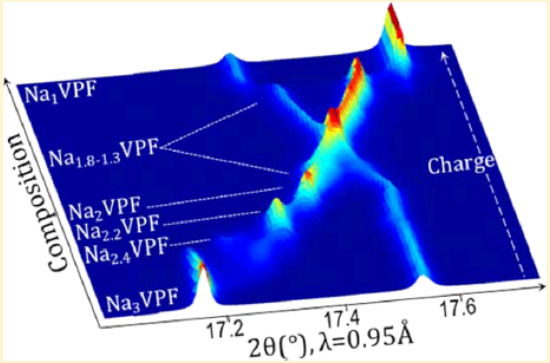

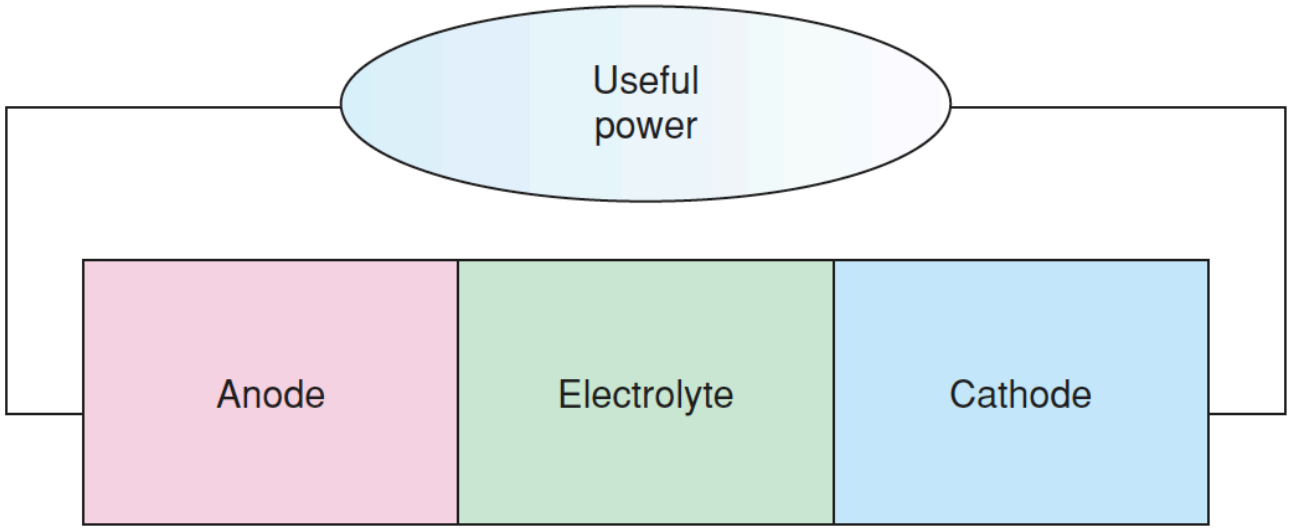

Anode	Electrolyte	Cathode
Li	$LiClO_4$/non-aq.	TiS_2
Li/Al	$LiClO_4$/polymer	V_6O_{13}
Li/C	Li^+ glass	Li_xCoO_2
	Li^+ ceramic	$Li_xMn_2O_4$

$$Ti^{4+}S_2 + xLi \rightarrow Li_x^+ Ti_{1-x}^{4+} Ti_x^{3+} S_2$$

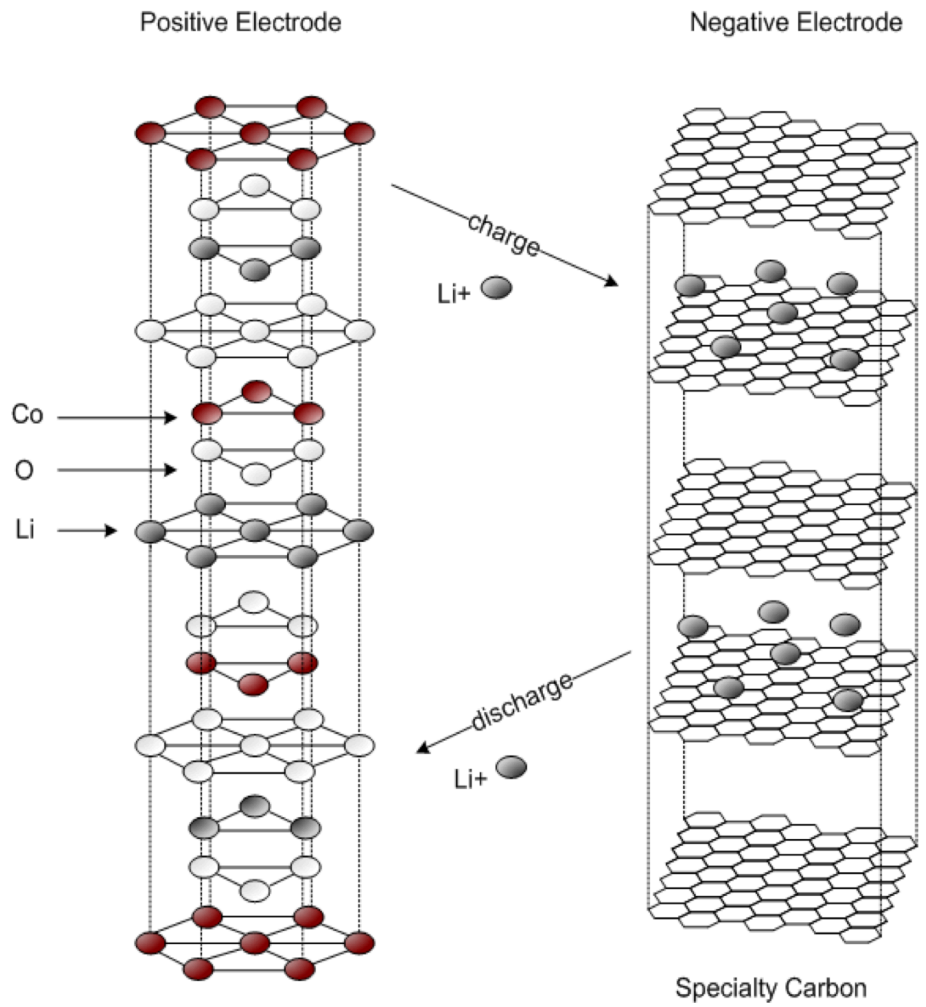

discharge ($\rightarrow$) and charge ($\leftarrow$) reactions

$$Li_xC \underset{\leftarrow}{\overset{\rightarrow}{}} C + xLi^+ + xe^- \quad (anode)$$

$$Li_{1-x}CoO_2 + xLi^+ + xe^- \underset{\leftarrow}{\overset{\rightarrow}{}} LiCoO_2 \quad (cathode)$$

Pros of sodium vs. lithium

- Lower price
- Great earth abundance

Cons:

- larger mass -> lower ion mobility
- Larger radius (Na^+ 1.2Å vs Li+ 0.7 Å)

- Less negative (-2.7 vs. -3.04V) std red potential

-> lower energy density

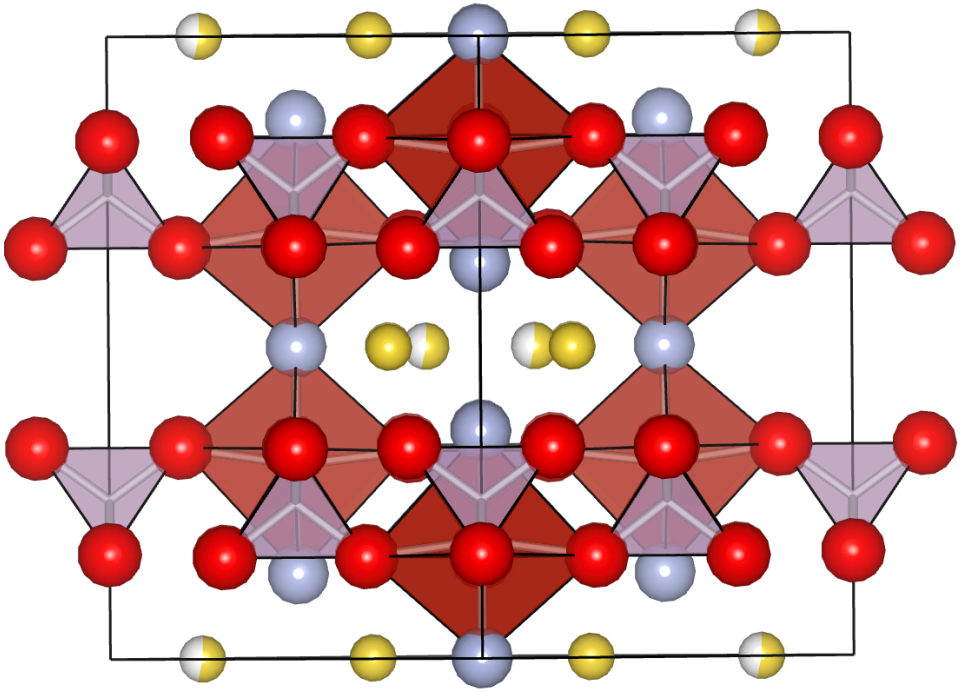

It is believed that lithium deintercalation proceeds through a “solid solution mechanism”:

- Continuous variation of lattice parameters in dependence on Na^+ concentration
- Same S.G: P4 2/m n m (tetragonal)

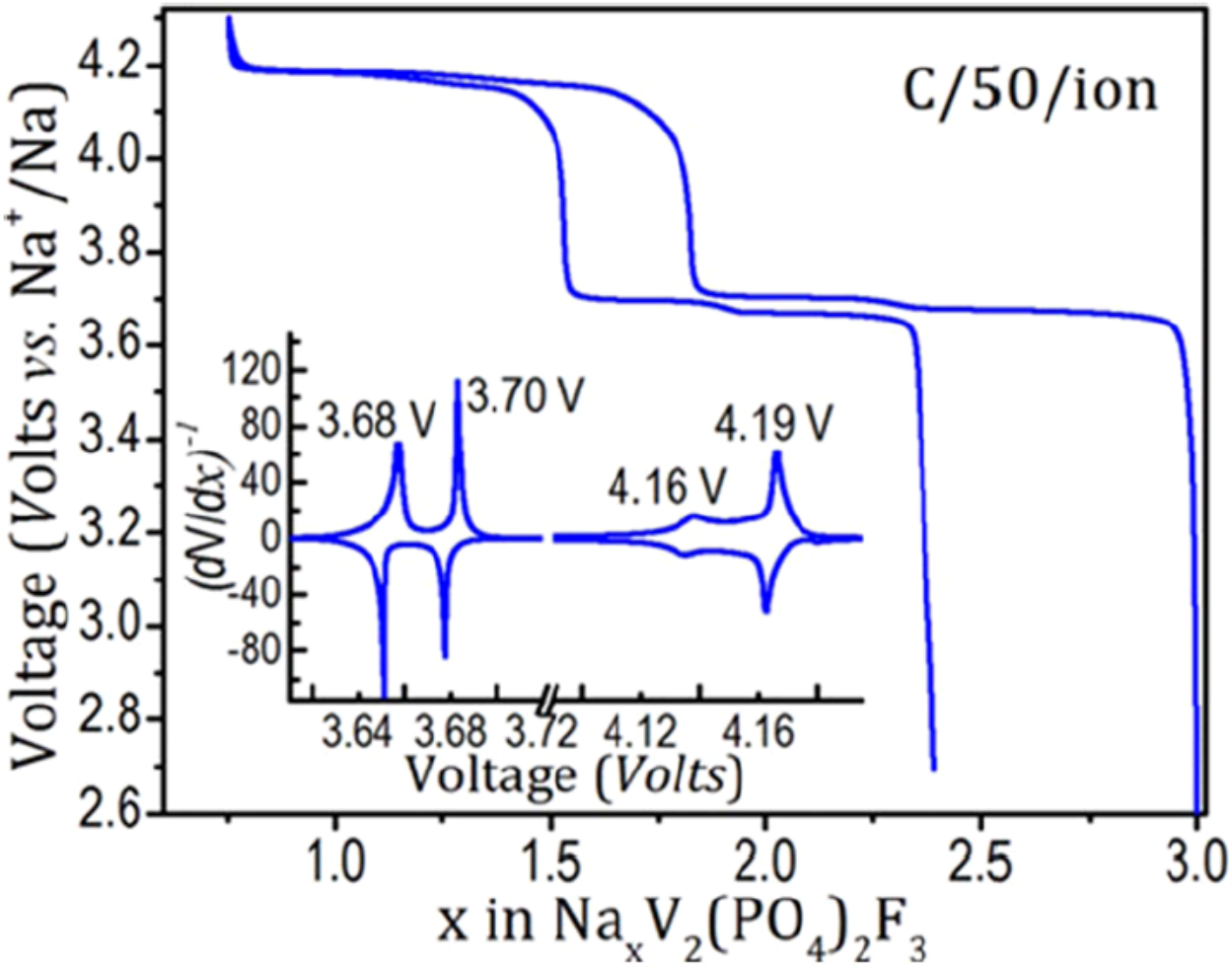

Figure 1. Galvanostatic electrochemical cycling of a $Na_3V_2(PO_4)_2F_3$// Na battery at C/50 rate per exchanged ion. Inset: Inverse derivative curve $(dV/dx)^{-1}$ showing the presence of several electrochemical features.


a)
Be
Main body
Screw
Plunger
1cm

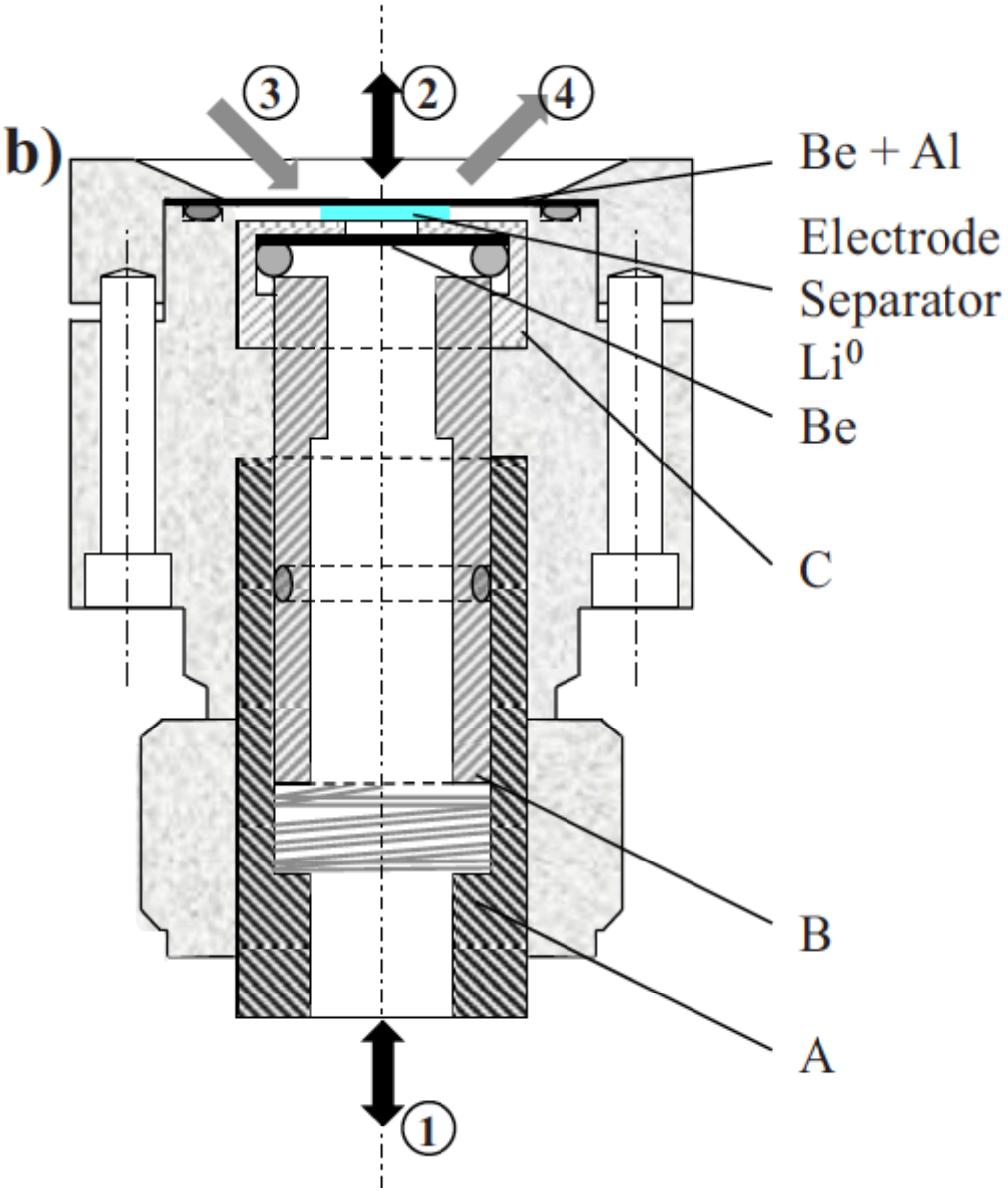
b)
3
2
4
Be + Al
Electrode
Separator
Li0
Be
C
B
A
1

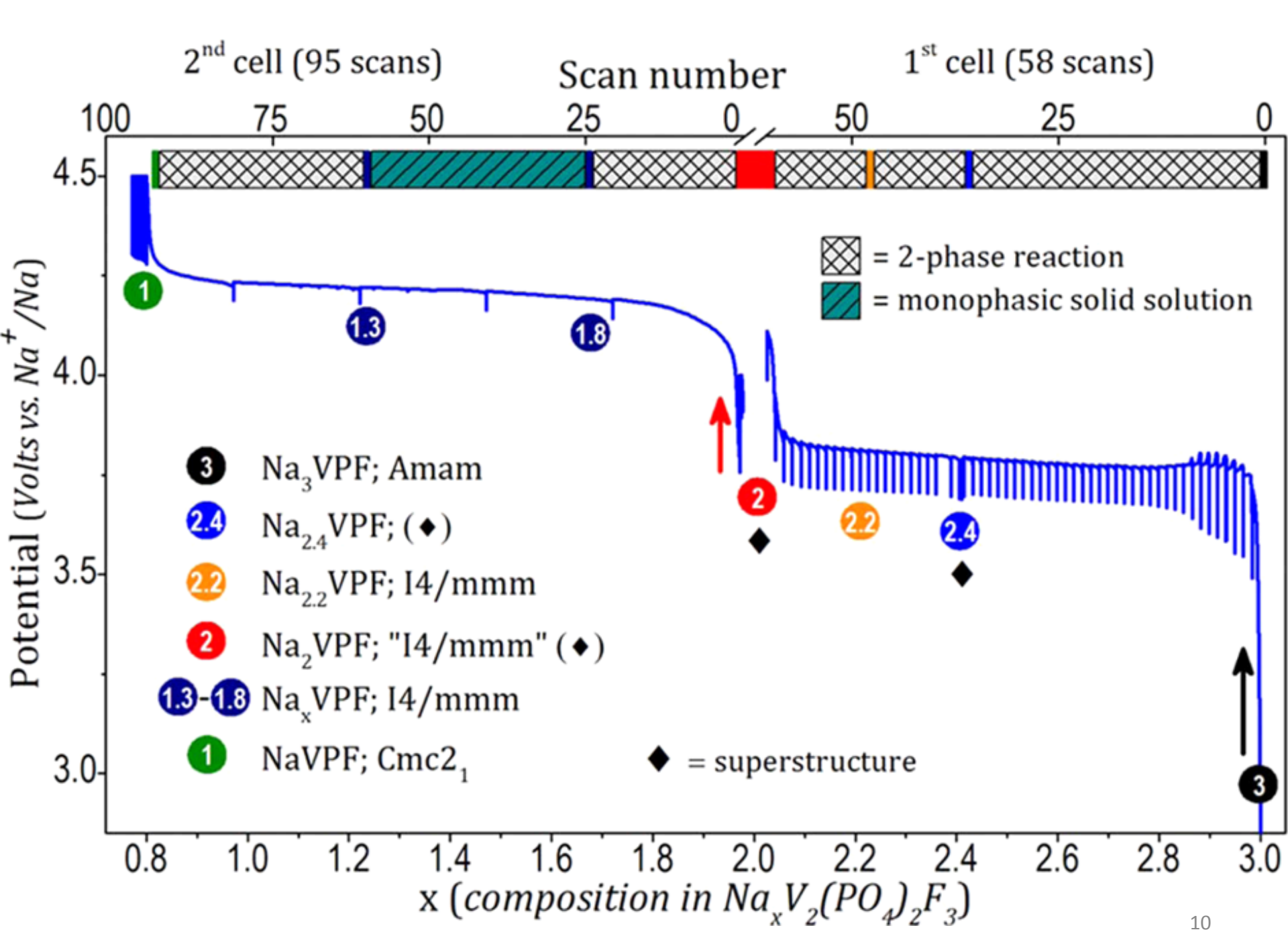
2nd cell (95 scans)
Scan number
1st cell (58 scans)
100
75
50
25
0
50
25
0
4.5
4.0
3.5
3.0
Potential (Volts vs. Na+/Na)
= 2-phase reaction
= monophasic solid solution
1
1.3
1.8
2
2.2
2.4
3
3 Na3VPF; Amam
2.4 Na2.4VPF; (◆)
2.2 Na2.2VPF; I4/mmm
2 Na2VPF; "I4/mmm" (◆)
1.3-1.8 NaxVPF; I4/mmm
1 NaVPF; Cmc21
◆ = superstructure
0.8
1.0
1.2
1.4
1.6
1.8
2.0
2.2
2.4
2.6
2.8
3.0
x (composition in NaxV2(PO4)2F3)

from $Na_3V_2(PO_4)_2F_3$ (N_3VPF) to $Na_2V_2(PO_4)_2F_3$ (N_2VPF)

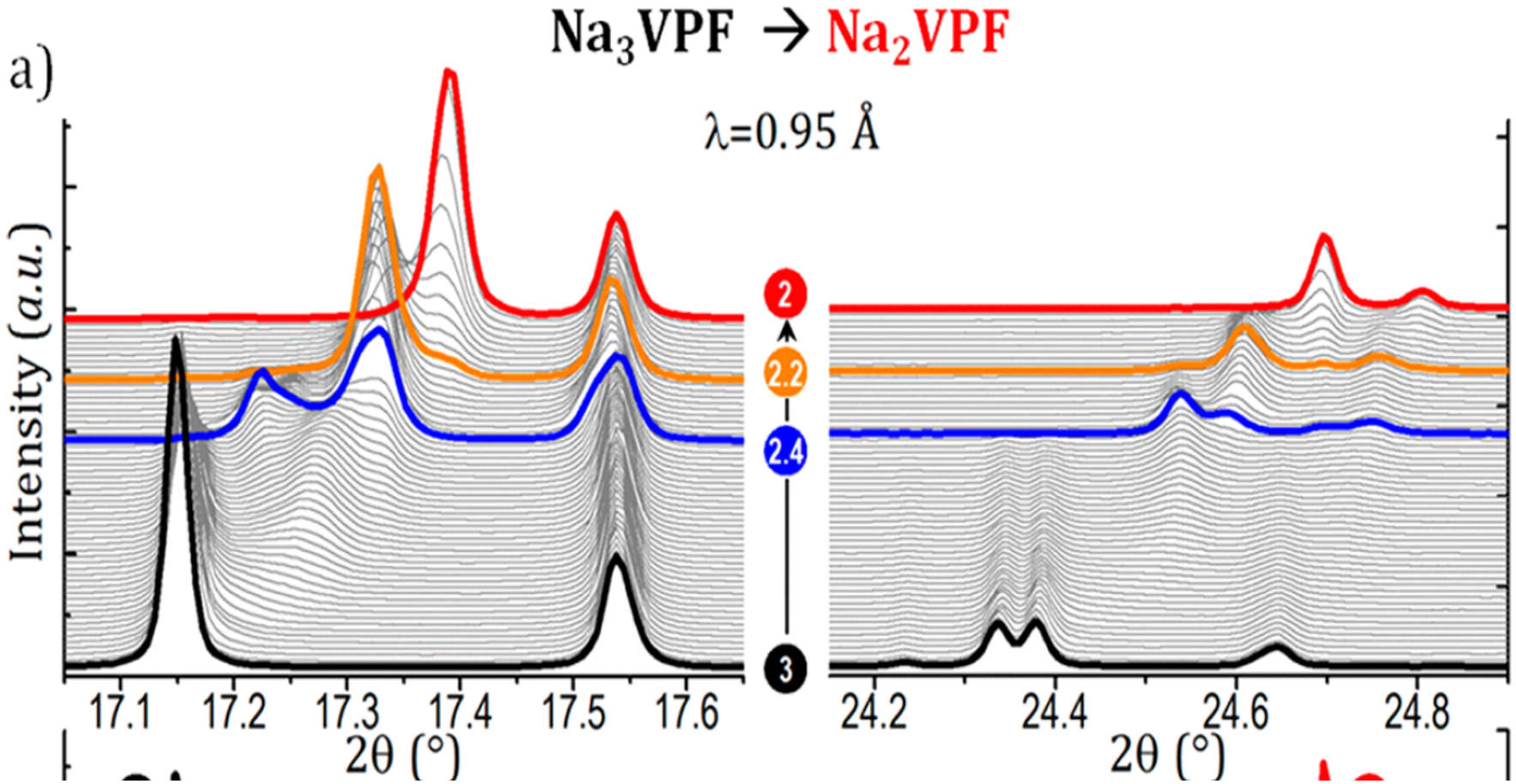

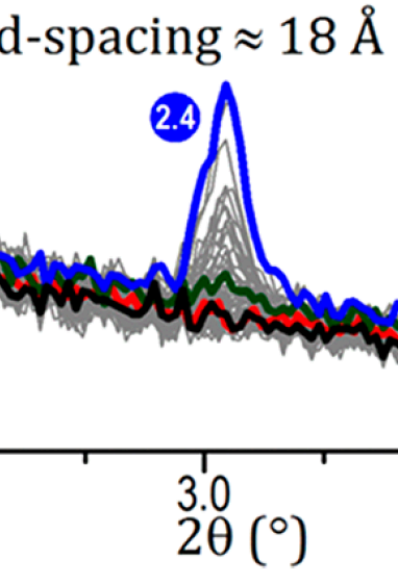
d-spacing ≈ 18 Å
2.4
3.0
2θ (°)

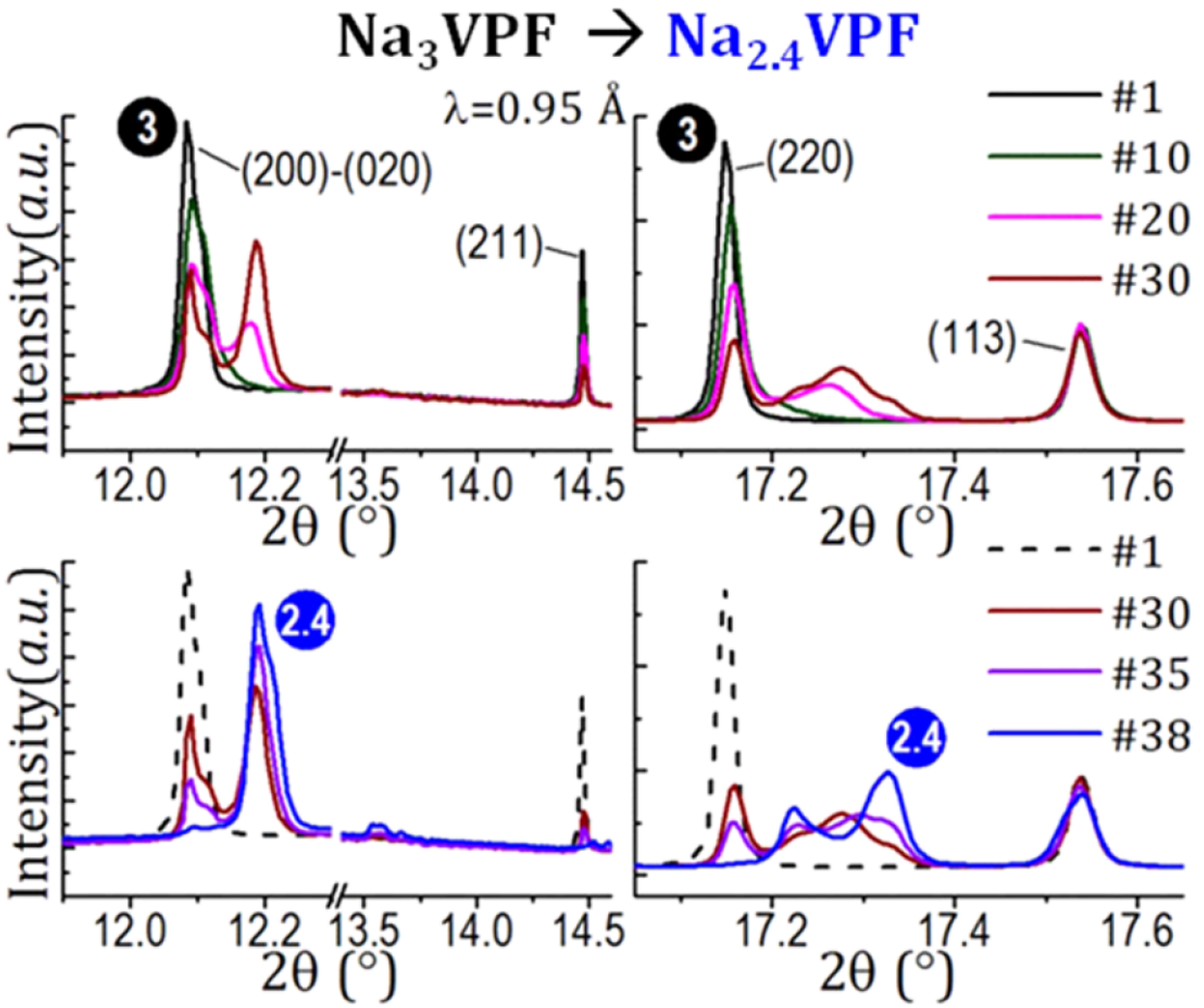
Na3VPF → Na2.4VPF
λ=0.95 Å
3
(200)-(020)
(211)
3
(220)
(113)
#1
#10
#20
#30
Intensity(a.u.)
12.0
12.2
13.5
14.0
14.5
17.2
17.4
17.6
2θ (°)
2.4
#1
#30
#35
#38

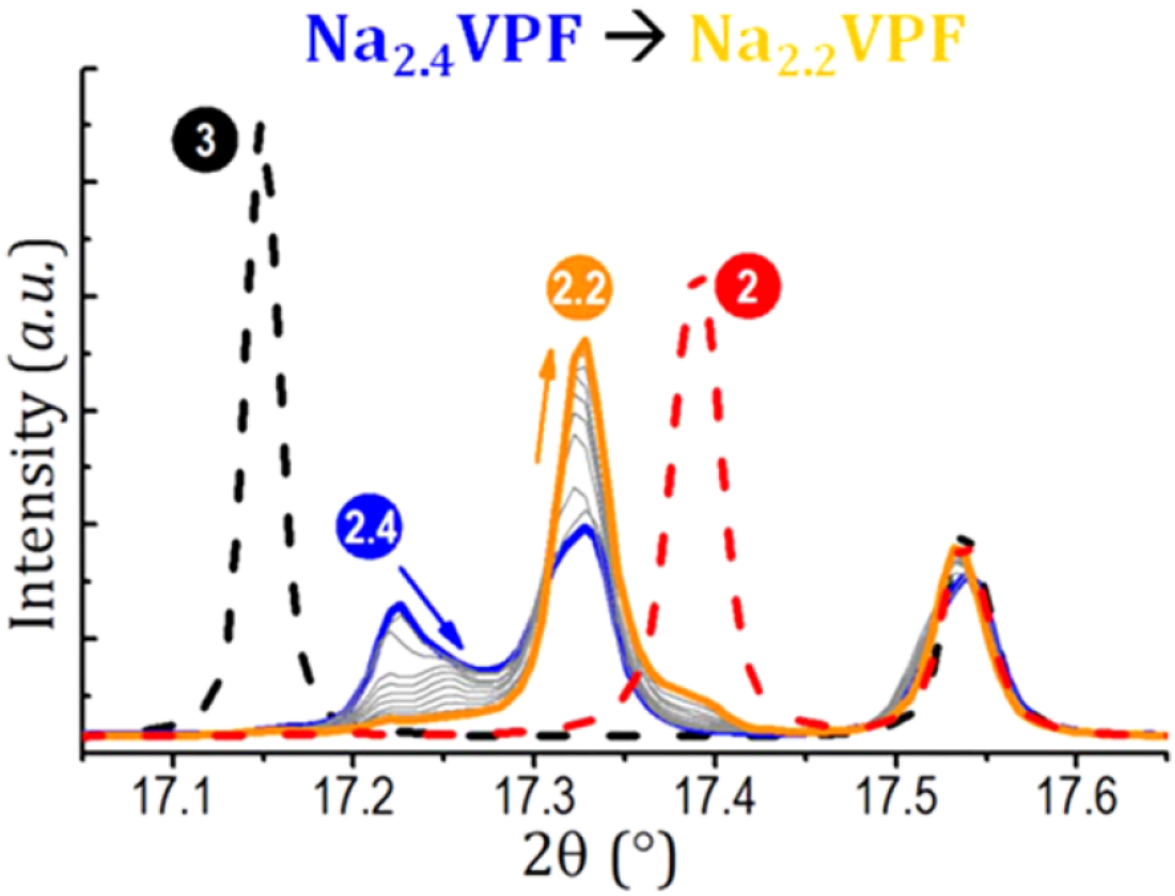

Figure 6. Detailed view of the biphasic reaction between scans no. 38 ($Na_{2.4}VPF$) and no. 47 ($Na_{2.2}VPF$). At this composition only two peaks at 17.33° and 17.54° remain, characteristic of the *I*4/*mmm* space group.

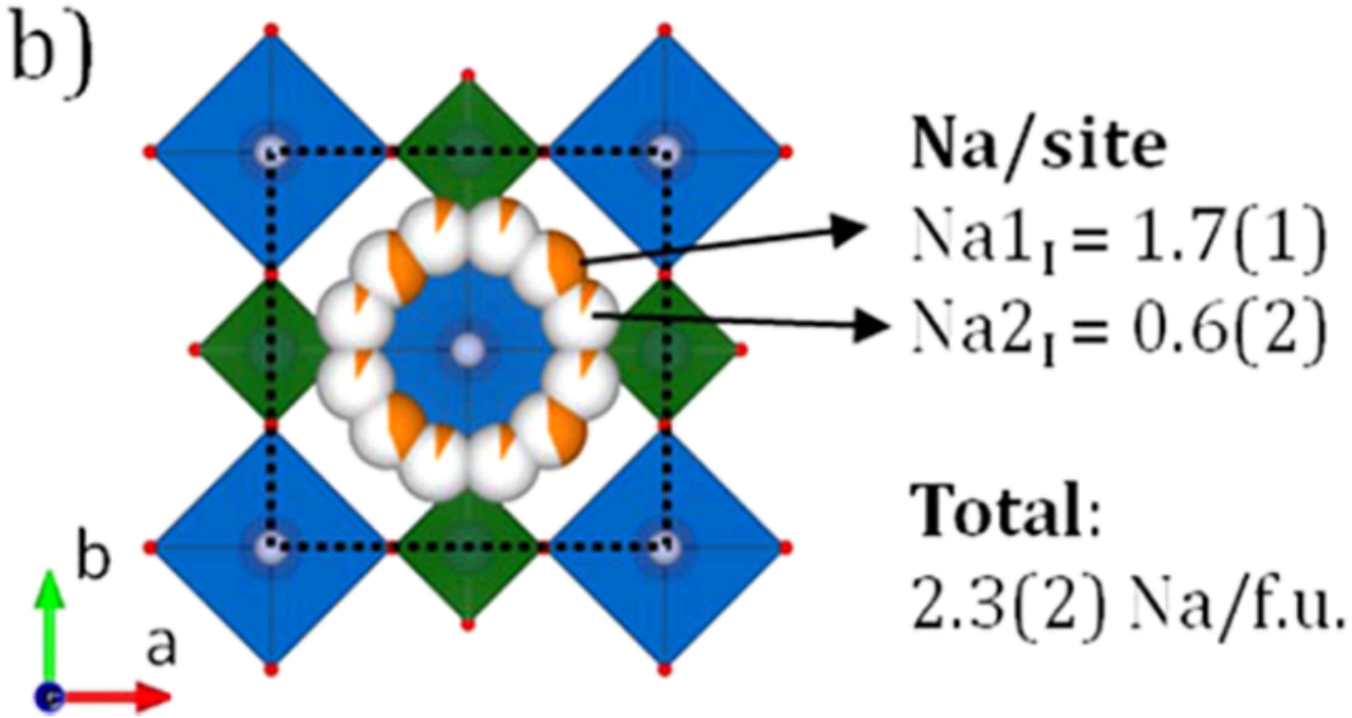

Figure 7. (a) Rietveld refinement of the intermediate phase $Na_{2.2}VPF$. Missing reflections related to sodium ordering in Na_3VPF (S.G.: *Amam*) are indicated by arrows. (b) Crystal structure of $Na_{2.2}VPF$, refined in the *I*4/*mmm* space group. Two sites $Na1_I$ and $Na2_I$ are present for sodium. Their occupancy is refined, and the related sodium amount is reported.

from $Na_2V_2(PO_4)_2F_3$ (N_2VPF) to $NaV_2(PO_4)_2F_3$ $(NVPF)$

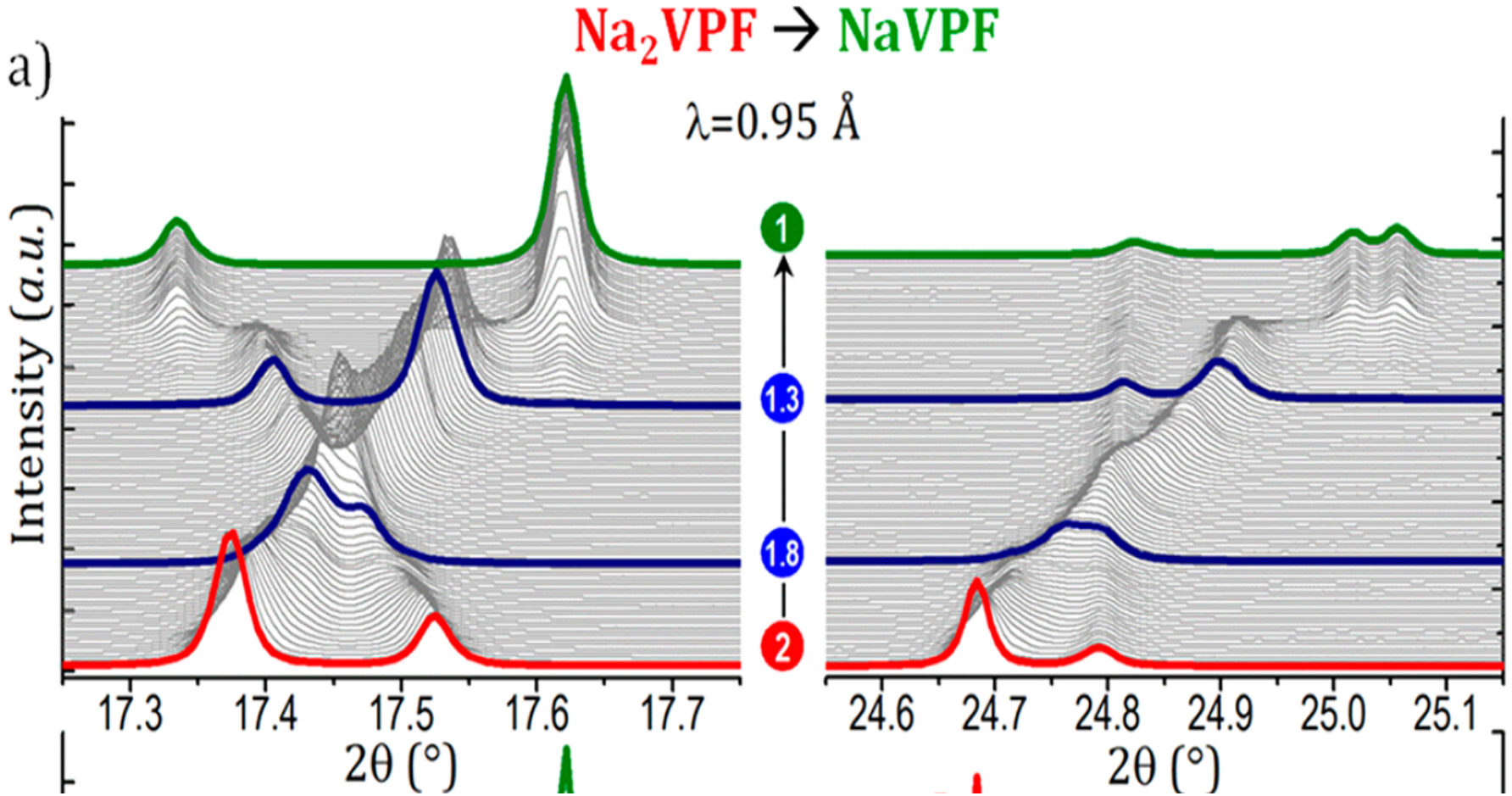

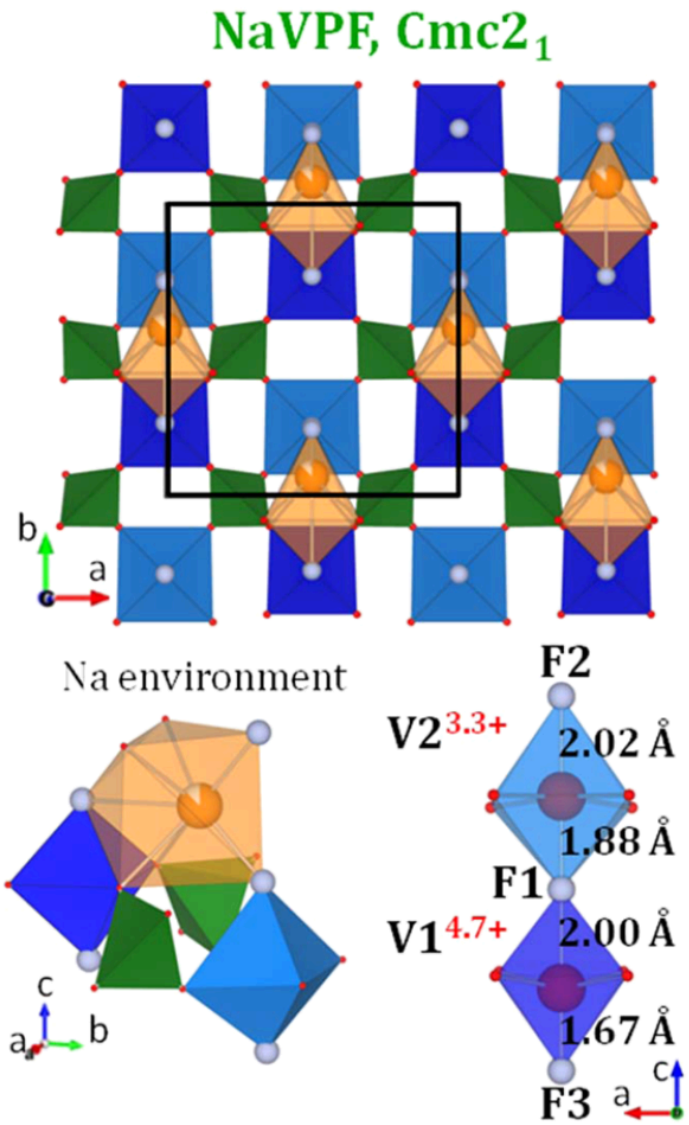

Figure 12. Structure of NaVPF (full composition $NaV_2(PO_4)_2F_3$) in the $Cmc2_1$ space group. Two different environments for vanadium cations are observed (dark and light blue), suggesting a V^{3+}–V^{5+} pair (oxidation state from BVS calculations is displayed). Environment of sodium in a capped prism is also reported.

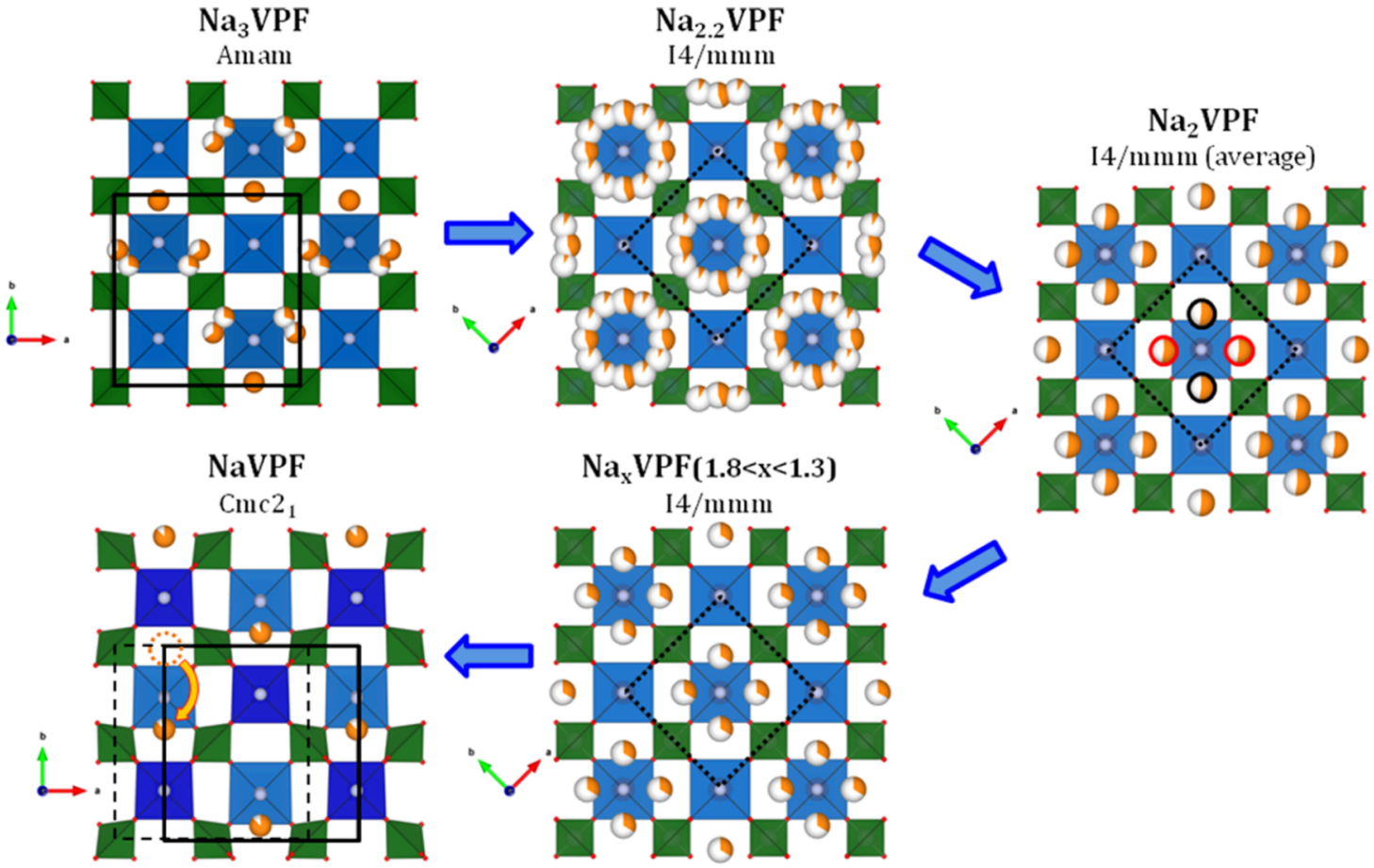

Figure 13. Sodium distribution obtained from Rietveld refinement of the different phases observed upon sodium extraction from Na_3VPF. Although a superstructure was observed for phase Na_2VPF, only the average structure was determined, thus the red/black circles indicate that only two positions out of four are expected to be occupied. For Na_1VPF, an orange dotted circle shows the second sodium site $Na1_A$ which is filled in the structure of Na_3VPF (dashed cell), while it is now empty.

Table 1. Compositions Obtained upon Na^+ Extraction from Na_3VPF[a]

composition	S. G.	*a* (Å)	*b* (Å)	*c* (Å)	vol. (Å^3)	*V*/*Z* (Å^3)
$Na_3V_2(PO_4)_2F_3$ (ref 26)	*Amam*	9.02847(3)	9.04444(3)	10.74666(6)	877.544(6)	219.386(6)
$Na_3V_2(PO_4)_2F_3$ (*in situ*)	*Amam*	9.0262(1)	9.0418(2)	10.7434(3)	876.80(1)	219.20(1)
$Na_{2.4}V_2(PO_4)_2F_3$		structure not determined				
$Na_{2.2}V_2(PO_4)_2F_3$	*I*4/*mmm*	6.3244(1)	6.3244(1)	10.7837(3)	431.33(1)	215.66(1)
$Na_2V_2(PO_4)_2F_3$	*I*4/*mmm* (average unit cell)	6.3021(1)	6.3021(1)	10.7933(2)	428.67(1)	214.34(1)
	Pmmm (considering a superstructure)[b]	25.221(1)	12.599(1)	21.586(1)	6859.42(3)	214.36(3)
$Na_{1.8}V_2(PO_4)_2F_3$ (solid sol.)	*I*4/*mmm*	6.2800(1)	6.2800(1)	10.8493(3)	427.88(1)	213.94(1)
$Na_{1.3}V_2(PO_4)_2F_3$ (solid sol.)		6.2481(1)	6.2481(1)	10.9222(2)	426.39(1)	213.19(1)
$NaV_2(PO_4)_2F_3$	$Cmc2_1$	8.7822(3)	8.7962(3)	11.0015(2)	849.86(1)	212.47(1)

[a]Space groups, cell parameters, and volumes are reported. [b]The actual space group of composition Na_2VPF in its superstructural arrangement is not known, so the low-symmetry space group *Pmmm* is used to index all observed reflections.

Table 2. Bond Lengths and Sodium Content/Formula Unit Obtained from Rietveld Refinement of Selected Deintercalated Phases Observed in Situ during Na^+ Extraction from Na_3VPF

composition	refined Na/f.u.	V−F1	V−F2	V−O1	V−O2
$Na_3V_2(PO_4)_2F_3$ (ref 26)	2.9(2)	1.981(2)	1.968(6)	2.006(9)	1.965(9)
$Na_3V_2(PO_4)_2F_3$ (in situ)	3.0(2)	1.985(3)	1.938(9)	2.00(1)	2.00(1)
$Na_{2.2}V_2(PO_4)_2F_3$	2.3(2)	1.953(5)	1.91(1)	1.954(6)	1.954(6)
$Na_2V_2(PO_4)_2F_3$ (*I*4/*mmm*)	2.05(7)	1.947(4)	1.88(1)	1.946(6)	1.946(6)
$Na_{1.8}V_2(PO_4)_2F_3$	1.85(7)	1.932(5)	1.92(1)	1.926(9)	1.926(9)
$Na_{1.3}V_2(PO_4)_2F_3$	1.31(6)	1.938(4)	1.87(1)	1.942(6)	1.942(6)
$NaV_2(PO_4)_2F_3$	0.88(9)	V1: 2.00(9)	V1−F3: 1.67(4)	V1−O1: 1.86(6)	V1−O2: 1.89(6)
		V2: 1.88(9)	V2−F2: 2.02(3)	V2−O3: 1.92(6)	V2−O4: 2.09(5)

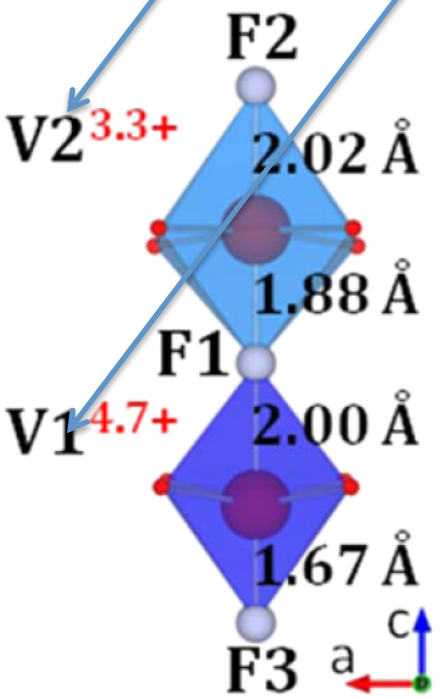

Case studies

- batteries
- **CO_2 capture by Chemical-Looping Combustion (CLC)**
- electrode-electrolyte interdiffusion processes
- *operando* Investigation of Fuel Cell

CHEMISTRY OF MATERIALS

Article

pubs.acs.org/cm

Oxygen Storage Properties of $La_{1-x}Sr_xFeO_{3-\delta}$ for Chemical-Looping Reactions—An In Situ Neutron and Synchrotron X-ray Study

Daniel D. Taylor,[†] Nathaniel J. Schreiber,[†,¶] Benjamin D. Levitas,[‡] Wenqian Xu,[§] Pamela S. Whitfield,[∥] and Efrain E. Rodriguez*[,†,‡]

[†]Department of Materials Science and Engineering, [‡]Department of Chemistry and Biochemistry, University of Maryland, College Park, Maryland 20742-2115, United States

[§]X-ray Science Division, Advanced Photon Source, Argonne National Laboratory, Argonne, Illinois 60439, United States

[∥]Spallation Neutron Source, Oak Ridge National Laboratory, Oak Ridge, Tennessee 37830, United States

Supporting Information

ABSTRACT: Oxygen storage materials (OSMs) provide lattice oxygen for a number of chemical-looping reactions including natural gas combustion and methane reforming. $La_{1-x}Sr_xFeO_{3-\delta}$ has shown promise for use as an OSM in methane reforming reactions due to its high product selectivity, fast oxide diffusion, and cycle stability. Here, we investigate the structural evolution of the series $La_{1-x}Sr_xFeO_{3-\delta}$ for x = 0, 1/3, 1/2, 2/3, and 1, using in situ synchrotron X-ray and neutron diffraction, as it is cycled under the conditions of a chemical-looping reactor (methane and oxygen atmospheres). In the compositions x = 1/3, 1/2, 2/3, and 1, we discover an "envelope", or temperature range, of oxygen storage capacity (OSC), where oxygen can easily and reversibly be inserted and removed from the OSM. Our in situ X-ray and neutron diffraction results reveal that while samples with higher Sr contents had a higher OSC, those same samples suffered from slower reaction kinetics and some, such as the x = 1/2 and x = 2/3 compositions, had local variations in Sr content, which led to inhomogeneous regions with varying reaction rates. Therefore, we highlight the importance of in situ diffraction studies, and we propose that these measurements are required for the thorough evaluation of future candidate OSMs. We recommend $La_{2/3}Sr_{1/3}FeO_{3-\delta}$ as the optimal OSM in the series because its structure remains homogeneous throughout the reaction, and its OSC "envelope" is similar to that of the higher doped materials.

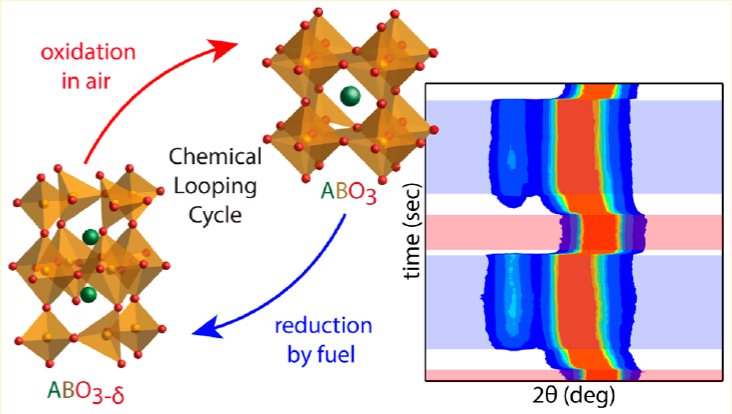

$M_yO_{x-1} + ½\ O_2(air) \rightarrow M_yO_x + (air : N_2 + unreacted\ O_2)$

$(2n + m)M_yO_x + C_nH_{2m} \rightarrow (2n + m)M_yO_{x-1} + mH_2O + nCO_2$

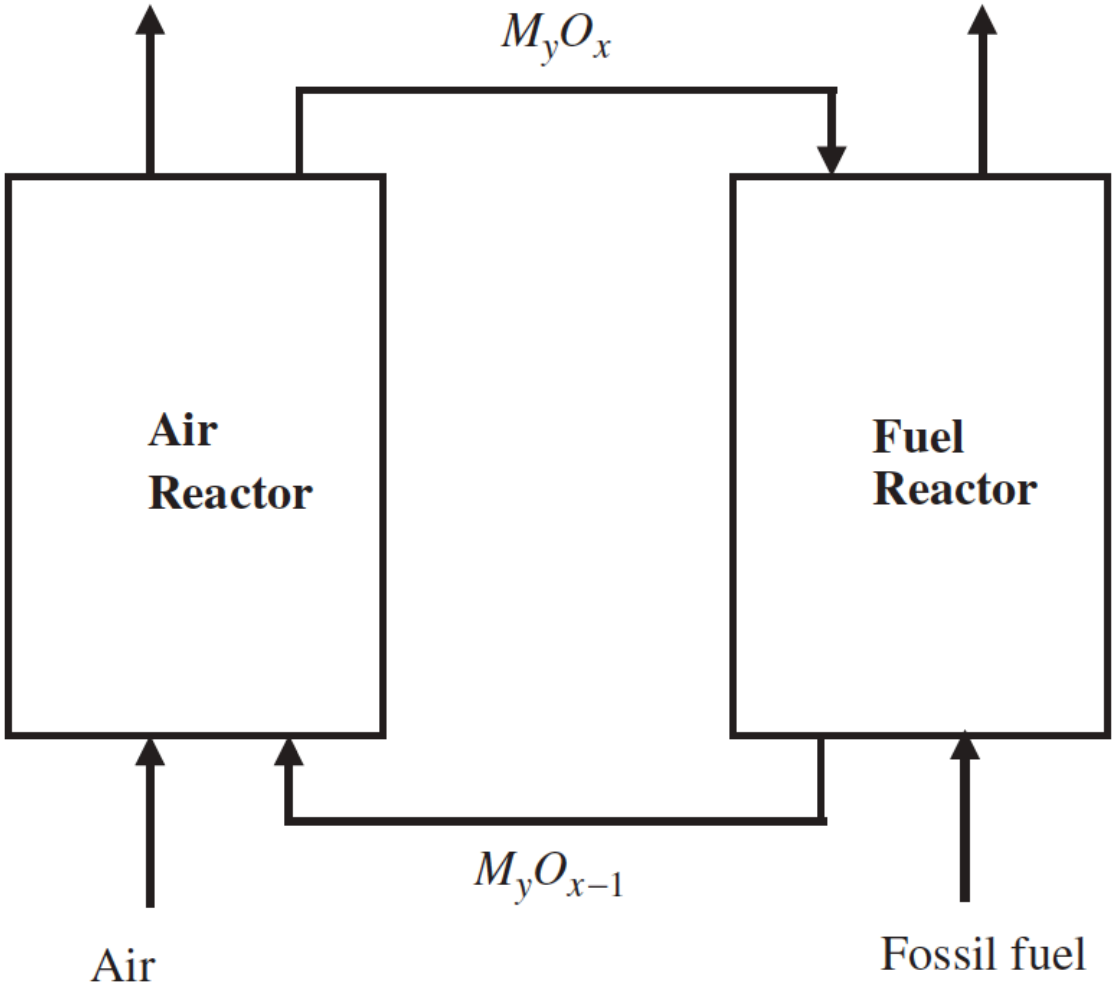

Control of the oxygen storage capacity:

Full oxidation: Chemical-looping combustion (CLC)

$$(2n + m)M_yO_x + C_nH_{2m} \rightarrow (2n + m)M_yO_{x-1} + mH_2O + nCO_2$$

Partial oxidation: Chemical-looping reforming (CLR)

$$CH_4 + M_yO_x \rightarrow CO + 2H_2 + M_yO_{x-1}$$

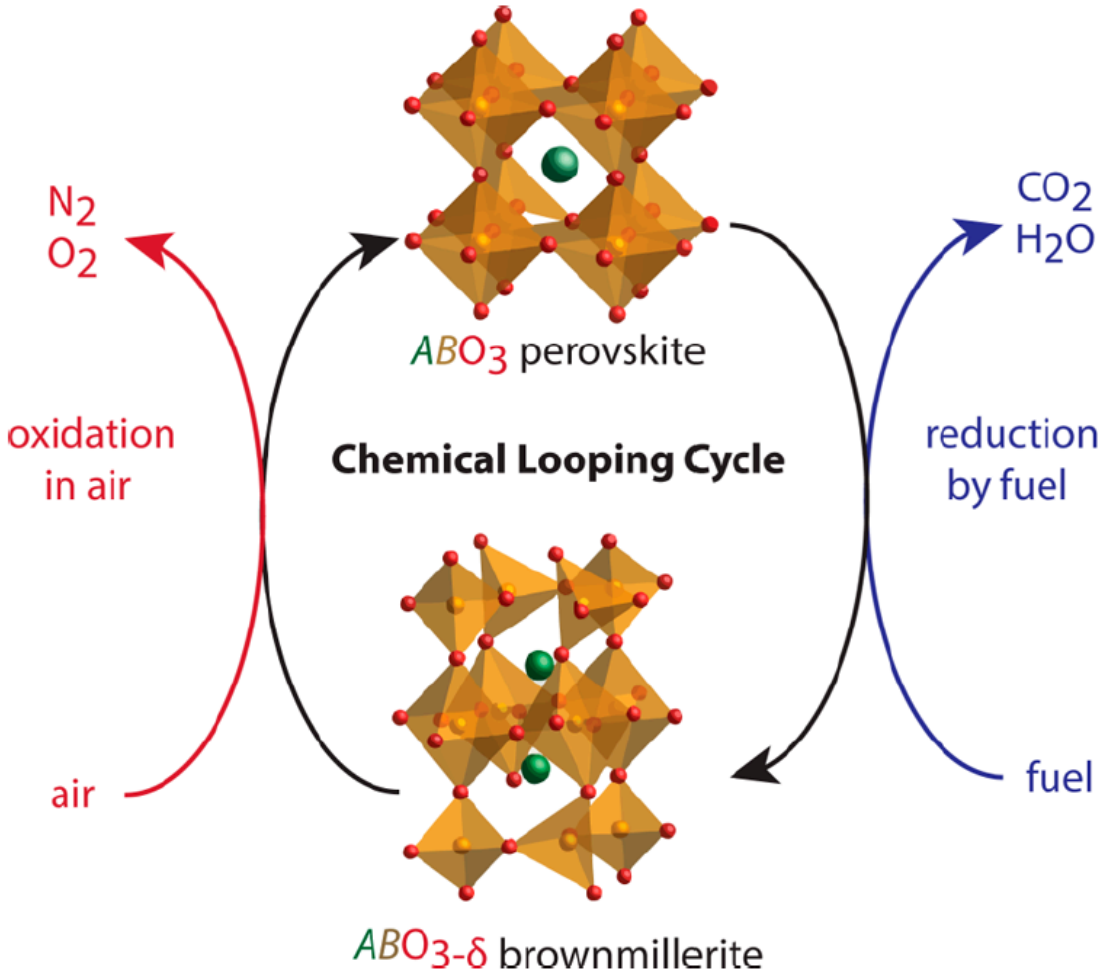

Figure 1. Schematic of the chemical-looping process. By selecting the oxygen storage material, it is possible to control the reaction products giving either pure CO_2 and H_2O (combustion), or CO and H_2 (reformation).

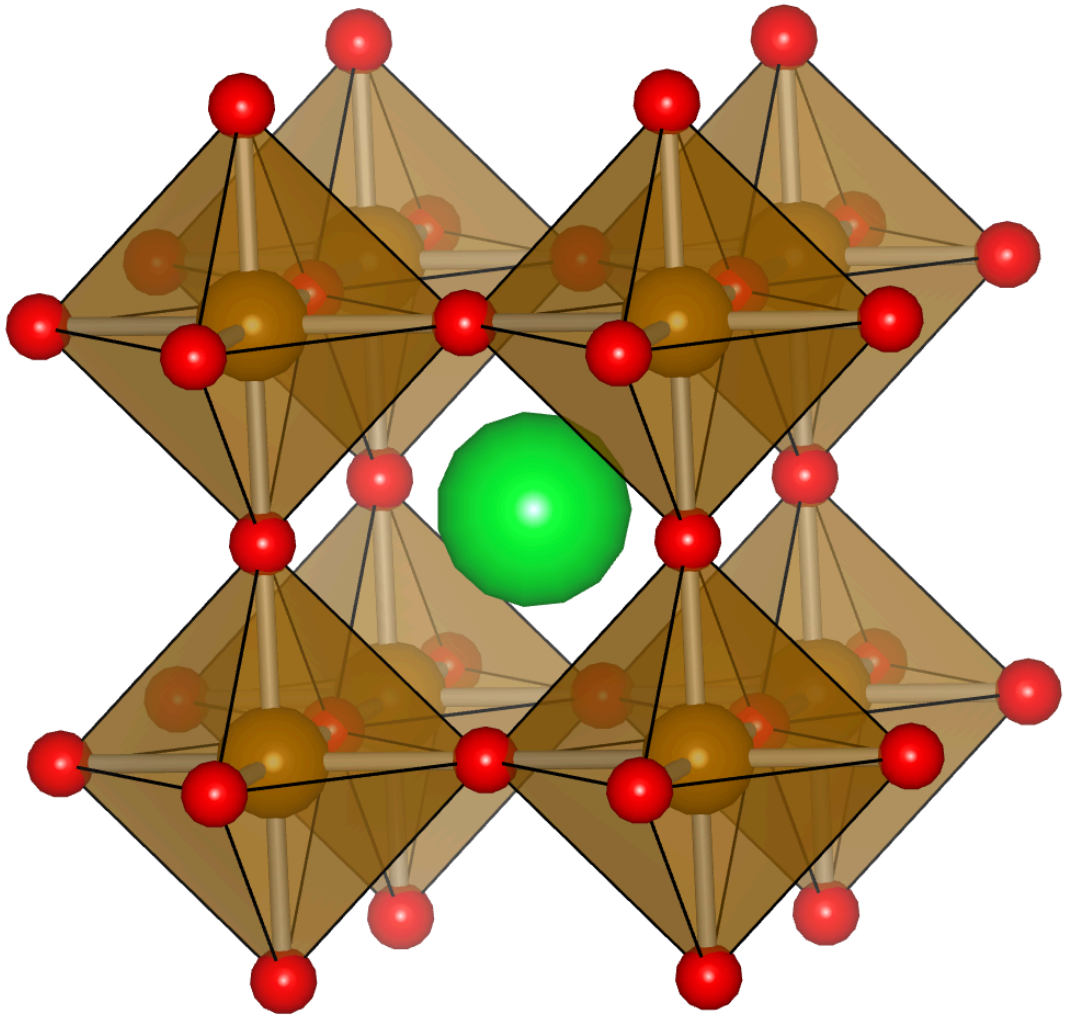

Pm-3m perovskite

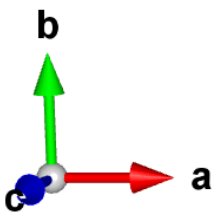

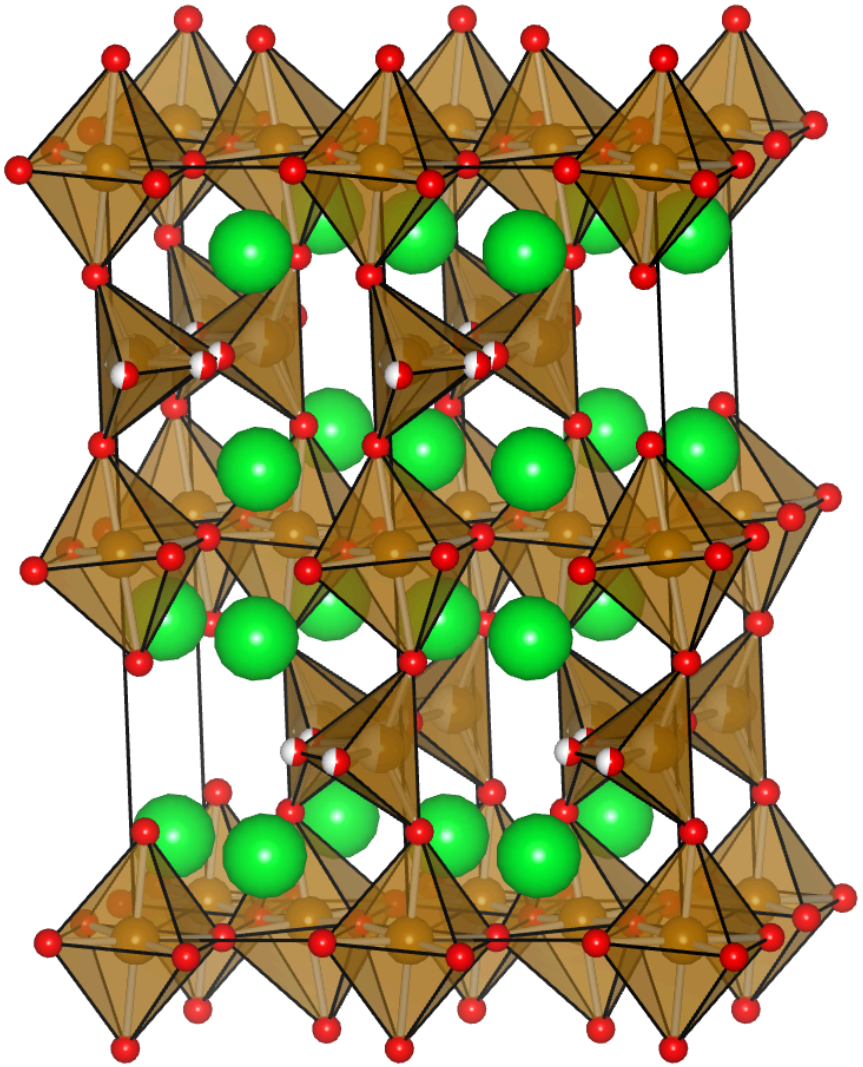

Icmm - brownmillerite

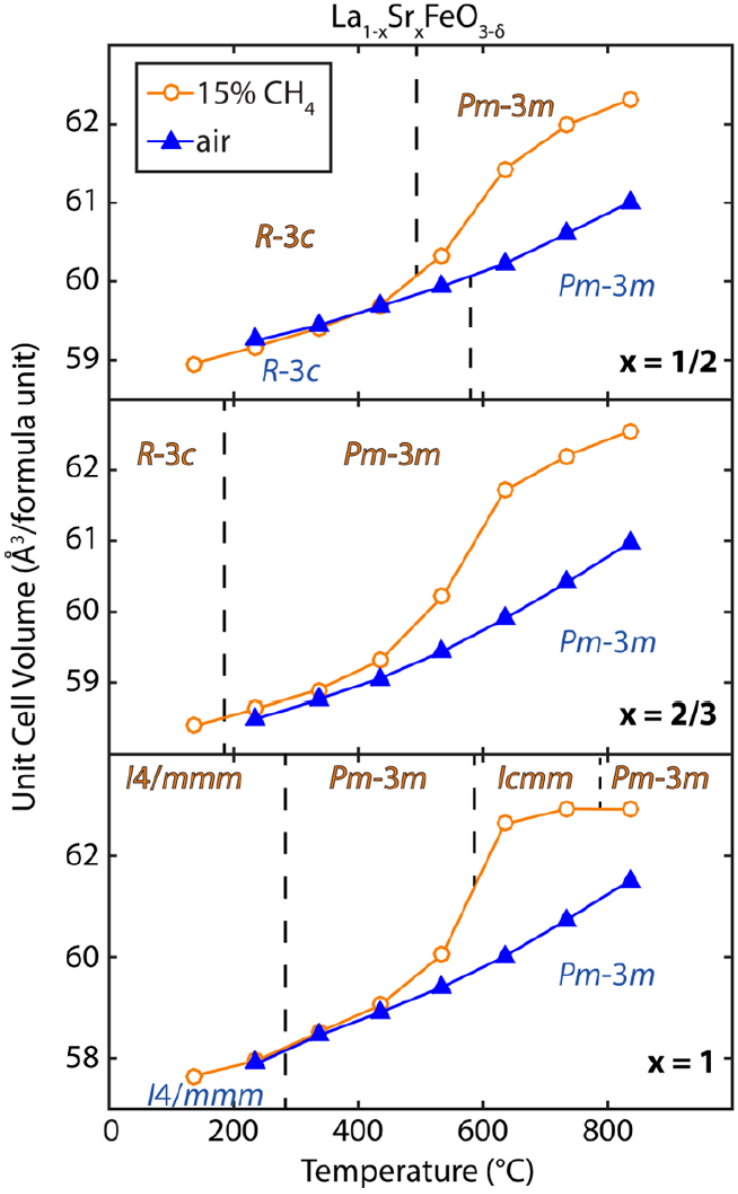
La1-xSrxFeO3-δ
15% CH4
air
Pm-3m
R-3c
Pm-3m
x = 1/2
R-3c
Pm-3m
Pm-3m
x = 2/3
I4/mmm
Pm-3m
Icmm
Pm-3m
Pm-3m
x = 1
I4/mmm
Unit Cell Volume (Å3/formula unit)
Temperature (°C)

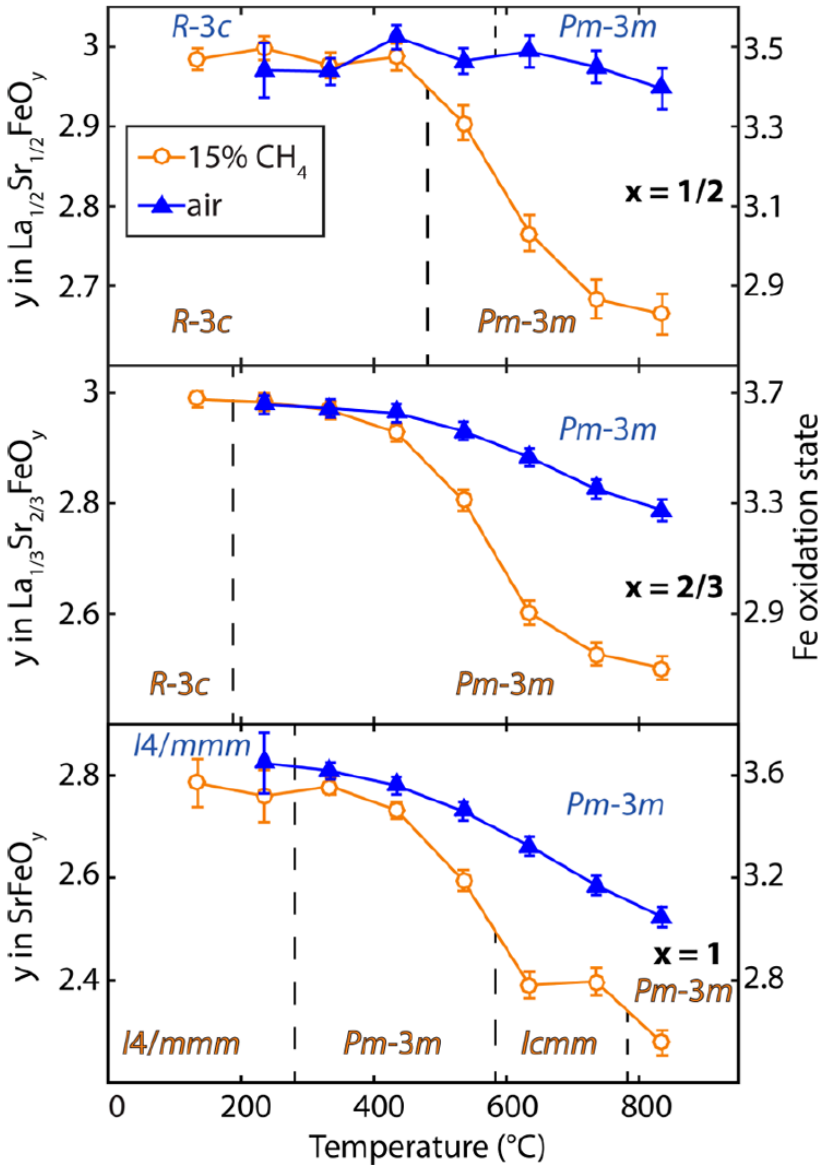
R-3c
Pm-3m
15% CH4
air
x = 1/2
R-3c
Pm-3m
y in La1/2Sr1/2FeOy
Pm-3m
x = 2/3
R-3c
Pm-3m
y in La1/3Sr2/3FeOy
I4/mmm
Pm-3m
x = 1
Pm-3m
I4/mmm
Pm-3m
Icmm
y in SrFeOy
Fe oxidation state
Temperature (°C)

NPD data

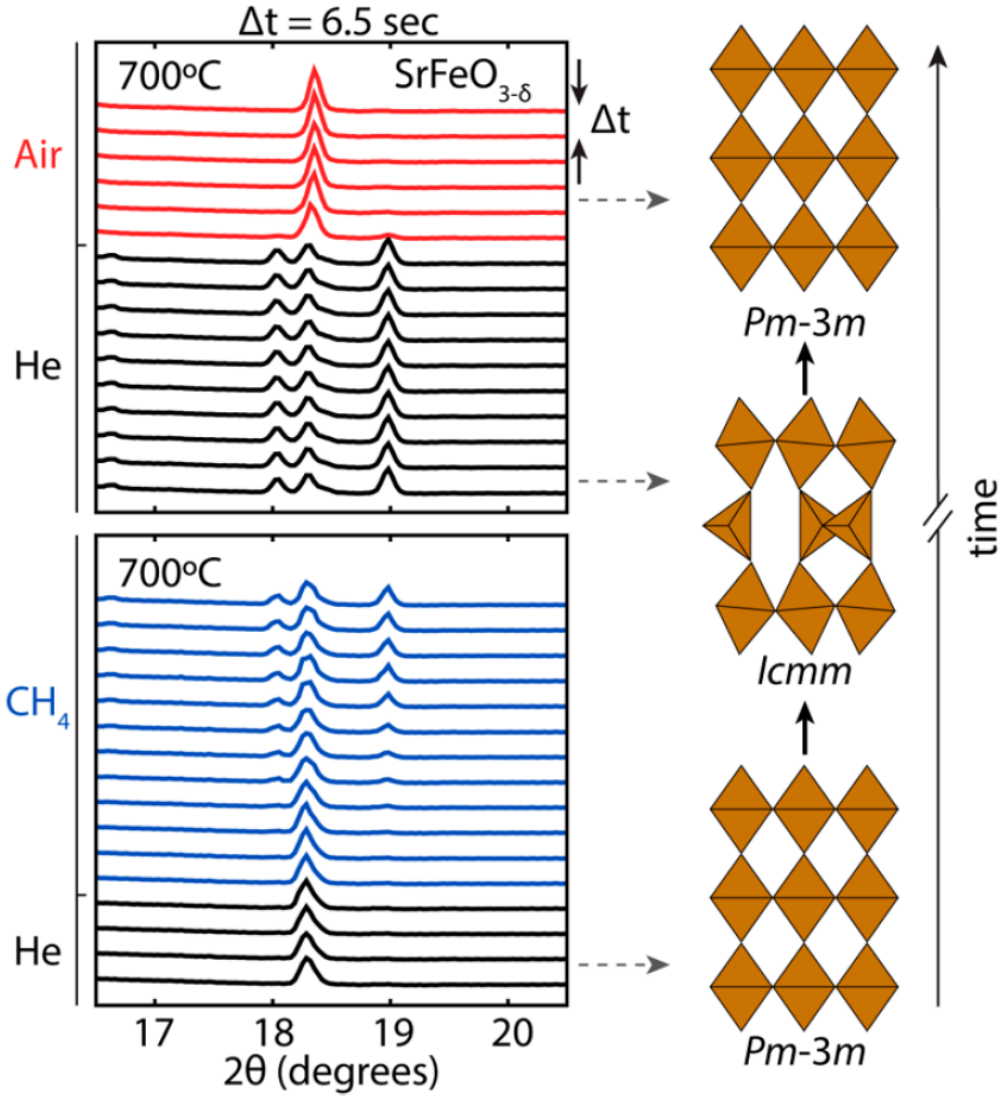

Figure 5. In situ SXRD (λ = 0.72768 Å) collected for $SrFeO_{3-\delta}$ at 700 °C as the atmosphere was cycled between helium, methane (15% CH_4/He), and air (20% O_2/He). Complete diffraction patterns were collected every 6.5 s. The crystal structures shown to the right represent the structure of the material at each step.

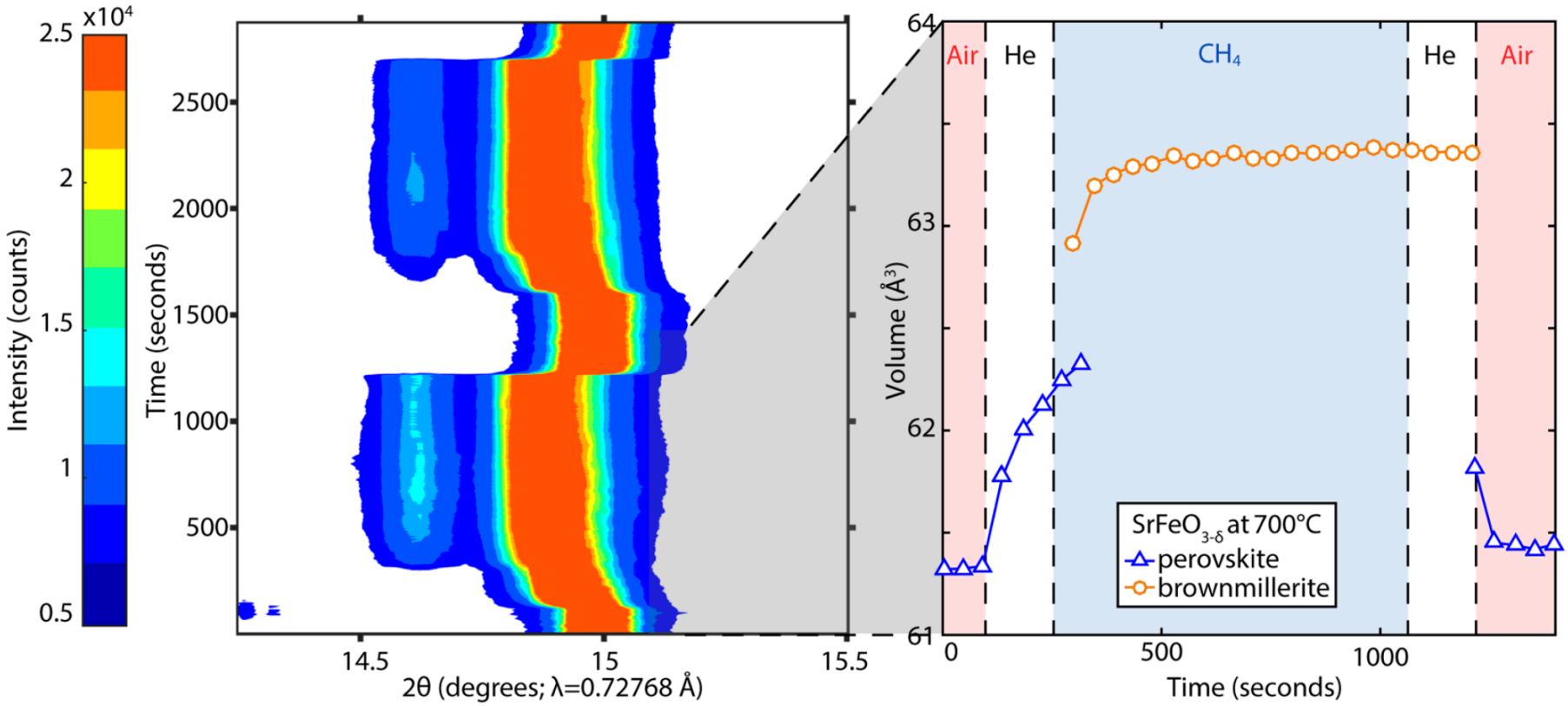

$SrFeO_{3-\delta}$ (x=1) structural evolution @700°C, 2 CH_4/air cycles

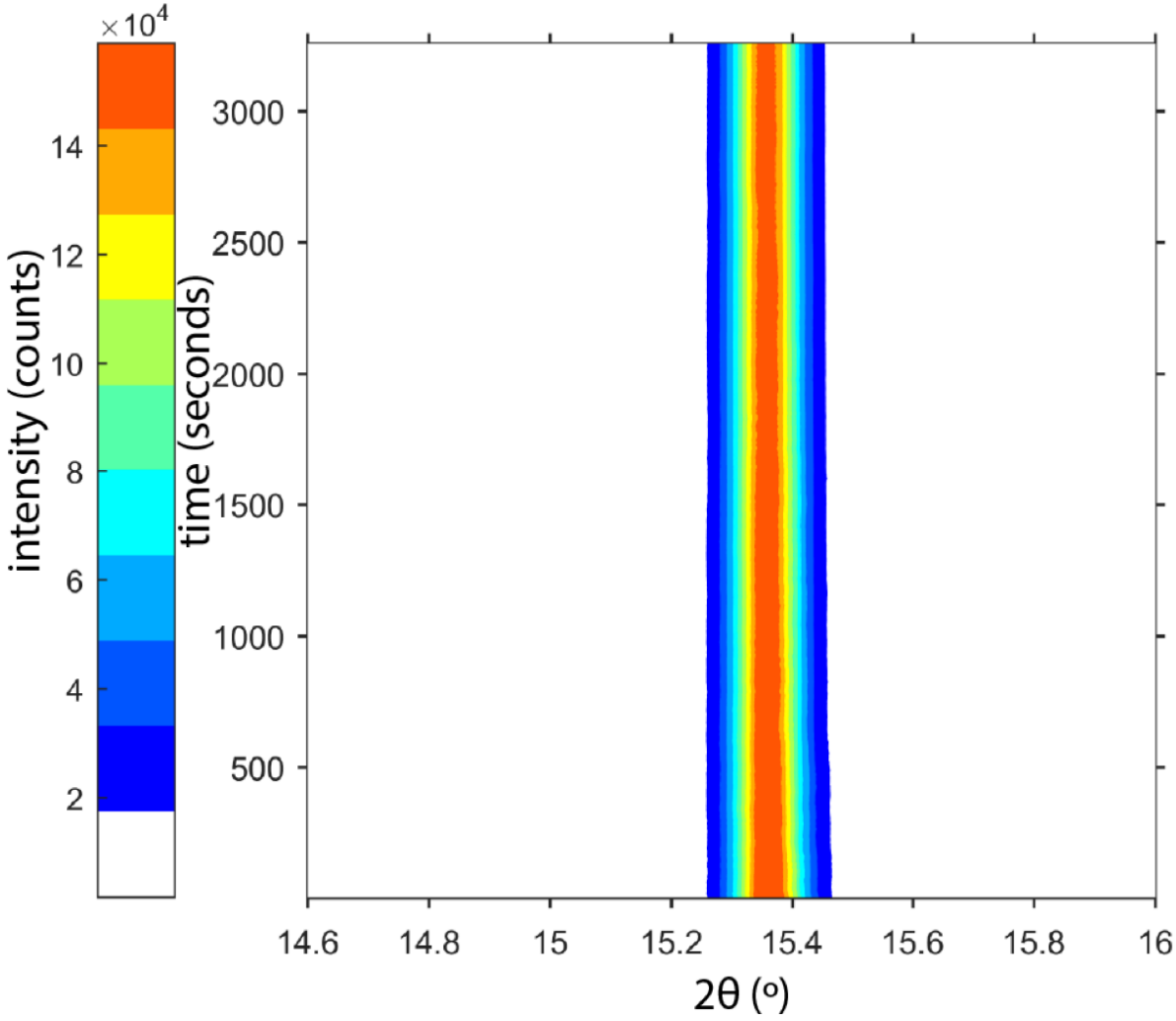

$LaFeO_3$ (x=0) does not release any oxygen

(large energy formation for an oxygen vacancy, about 4-5 eV)

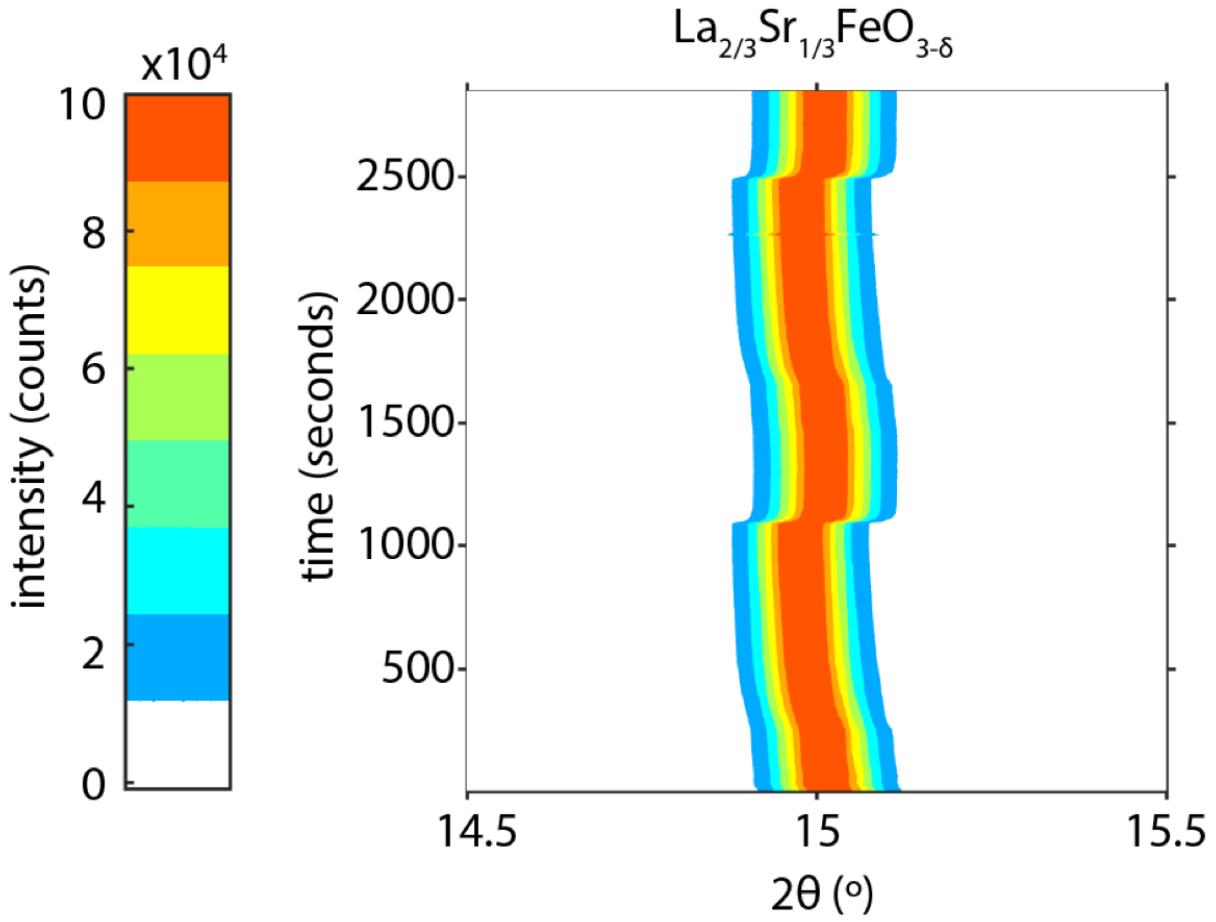

Figure S15. Contour plot of $La_{2/3}Sr_{1/3}FeO_{3-\delta}$ from synchrotron X-ray diffraction data for two complete cycles at 700°C (λ = 0.72768 Å).

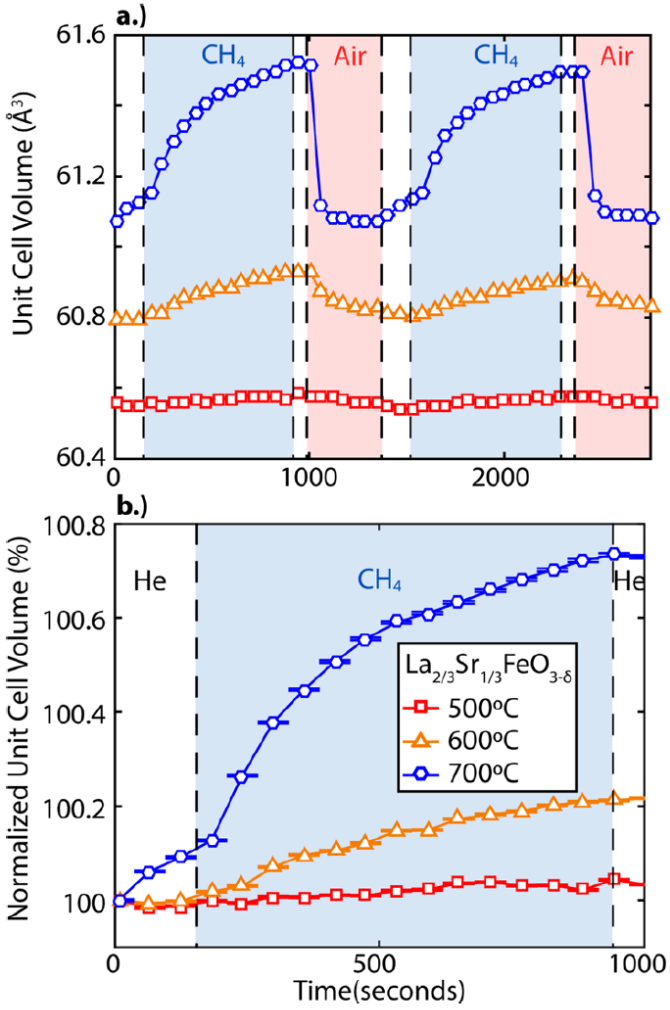

Figure 7. (a) Refined unit cell volume, normalized by formula unit, from in situ SXRD experiments for $La_{2/3}Sr_{1/3}FeO_{3-\delta}$ for two complete cycles at 500, 600, and 700 °C. (b) The normalized unit cell volume expansion. Error bars for the volume were obtained from the standard uncertainty from the Rietveld refinement but are smaller than the markers.

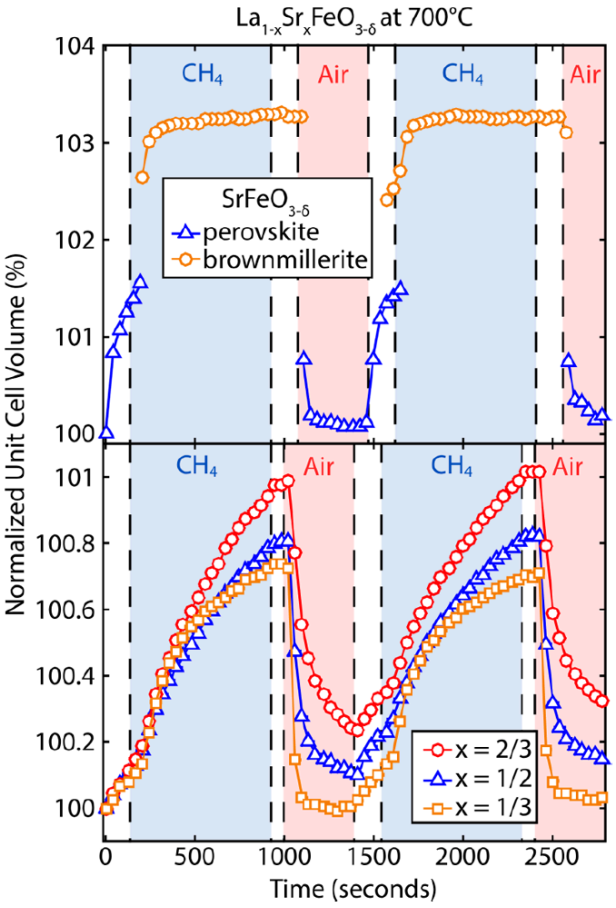

Figure 9. Normalized unit cell volume for two complete cycles of $La_{1-x}Sr_xFeO_{3-\delta}$ for x = 1/3, 1/2, 2/3, and 1 at 700 °C—data from in situ SXRD. $SrFeO_{3-\delta}$ had the largest unit cell expansion when reduced (>3%) and the shortest reaction time. Furthermore, $SrFeO_{3-\delta}$ transitioned between the perovskite and brownmillerite structures with cycling, whereas the others remained in the perovskite structure throughout the cycle. Only $La_{2/3}Sr_{1/3}FeO_{3-\delta}$ and $SrFeO_{3-\delta}$ completely reoxidized before the beginning of the second reduction step. Error bars for the volume were obtained from the standard uncertainty from the Rietveld refinement but are smaller than the markers.

Table 2. Oxygen Storage Properties of Select Complex Transition Metal Oxides and Their Reaction Conditions

	conditions		oxygen storage capacity		
compound	temperatures	cycling atmospheres	wt %	mmol O_2/gram	reference
$BaYMn_2O_{5+\delta}$	300 to 600 °C	5% H_2 and 100% O_2	3.7	1.2	38
$Dy_{0.7}Y_{0.3}MnO_{3+\delta}$	200 to 400 °C	air and 100% O_2	2.0	0.62	39
$HoMnO_{3+\delta}$	300 °C	air and 100% O_2	1.7	0.54	40
$Sr_3Fe_2O_{7-\delta}$	950 °C	5% H_2 and air	2.0	0.62	41
$La_{0.5}Sr_{0.5}Co_{0.5}Fe_{0.5}O_{3-\delta}$	400 to 600 °C	5% H_2 and air	3.6	1.1	42
$BaYCo_4O_{7+\delta}$	350 °C	N_2 and 100% O_2	3.5	1.1	43, 44
$LuFe_2O_{4+\delta}$	200 to 400 °C	5% H_2 and 2×10^{-4} atm pO_2	2.2	0.69	45
$Ca_2(Al_xMn_{1-x})_2O_{5+\delta}$	300 to 700 °C	100% N_2 and 100% O_2	3.0	0.94	46
$Ce_{0.7}Cu_{0.3}O_{2+\delta}$	700 °C	5% H_2 and air	3.2	1.0	47
$La_{1-x}Sr_xFeO_{3+\delta}$	600 to 835 °C	15% methane and air	2.3	0.7	this work

Case studies

- batteries
- CO_2 capture by Chemical-Looping Combustion (CLC)
- **electrode-electrolyte interdiffusion processes**
- *operando* investigation of Fuel Cell

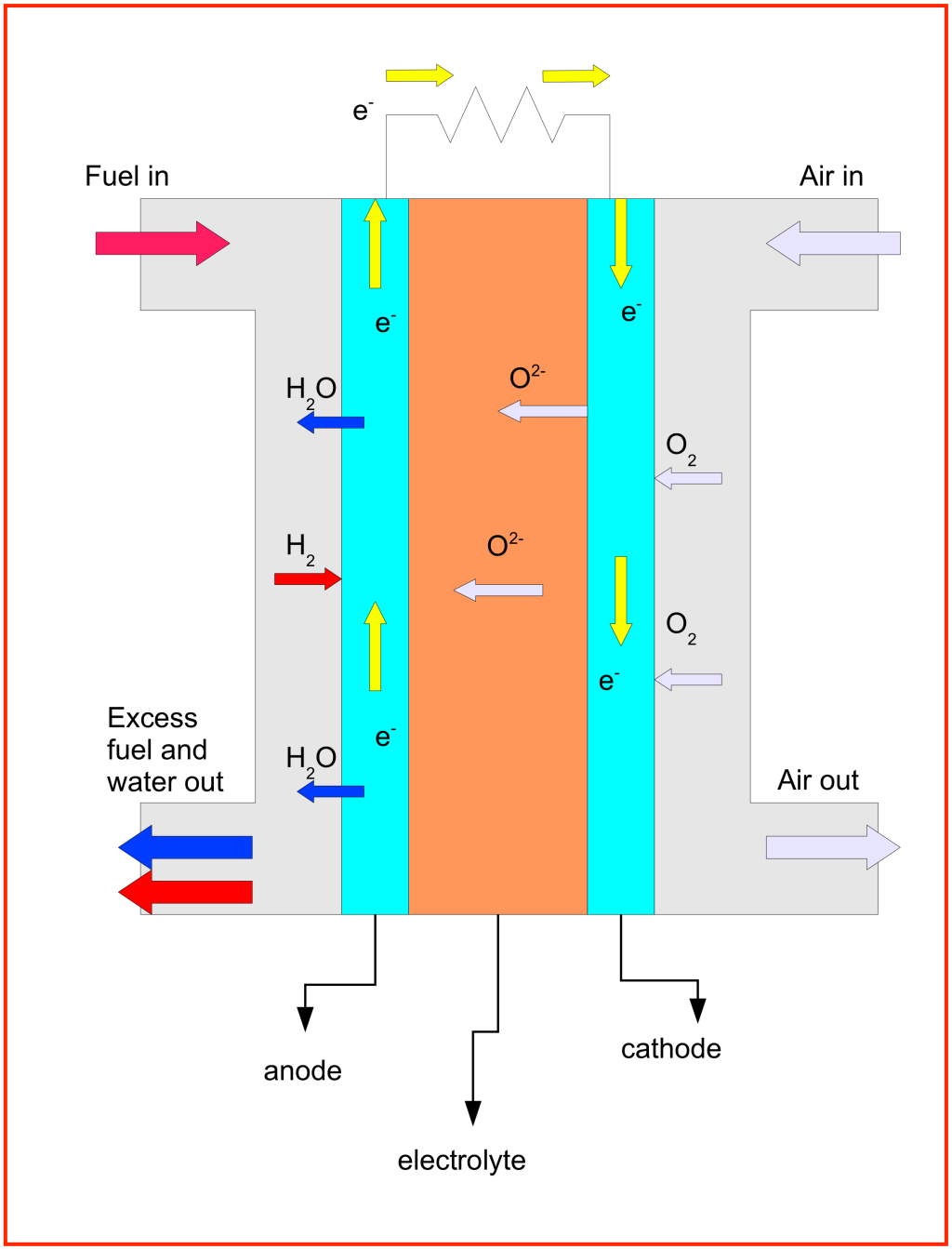

Anode reaction
$2H_2 \rightarrow 4H^+ + 4e^-$

Cathode reaction
$O_2 + 4e^- \rightarrow 2O^{2-}$

Overall reaction
$O_2 + 2H_2 \rightarrow 2H_2O$

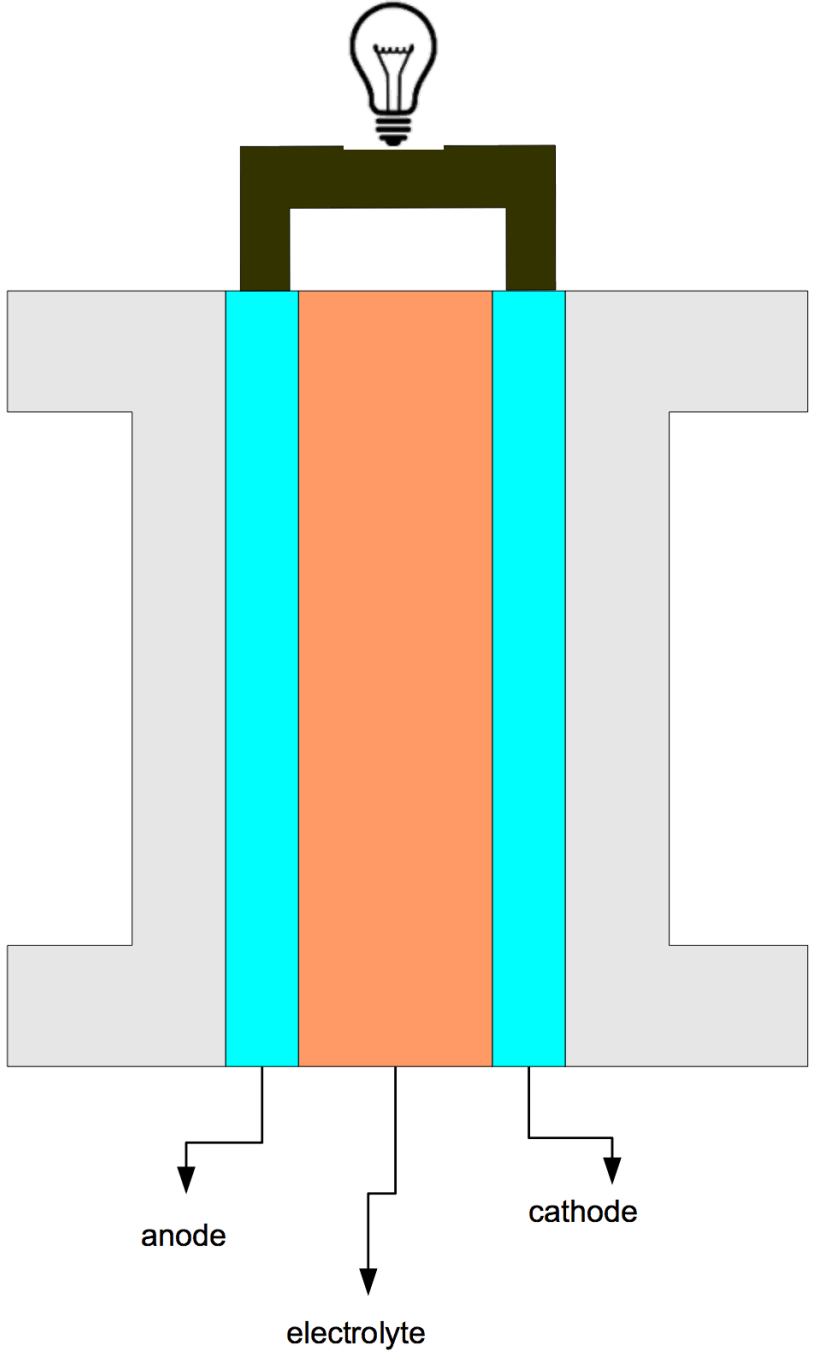
anode
electrolyte
cathode

Scanning X-Ray Microscope (ID21)

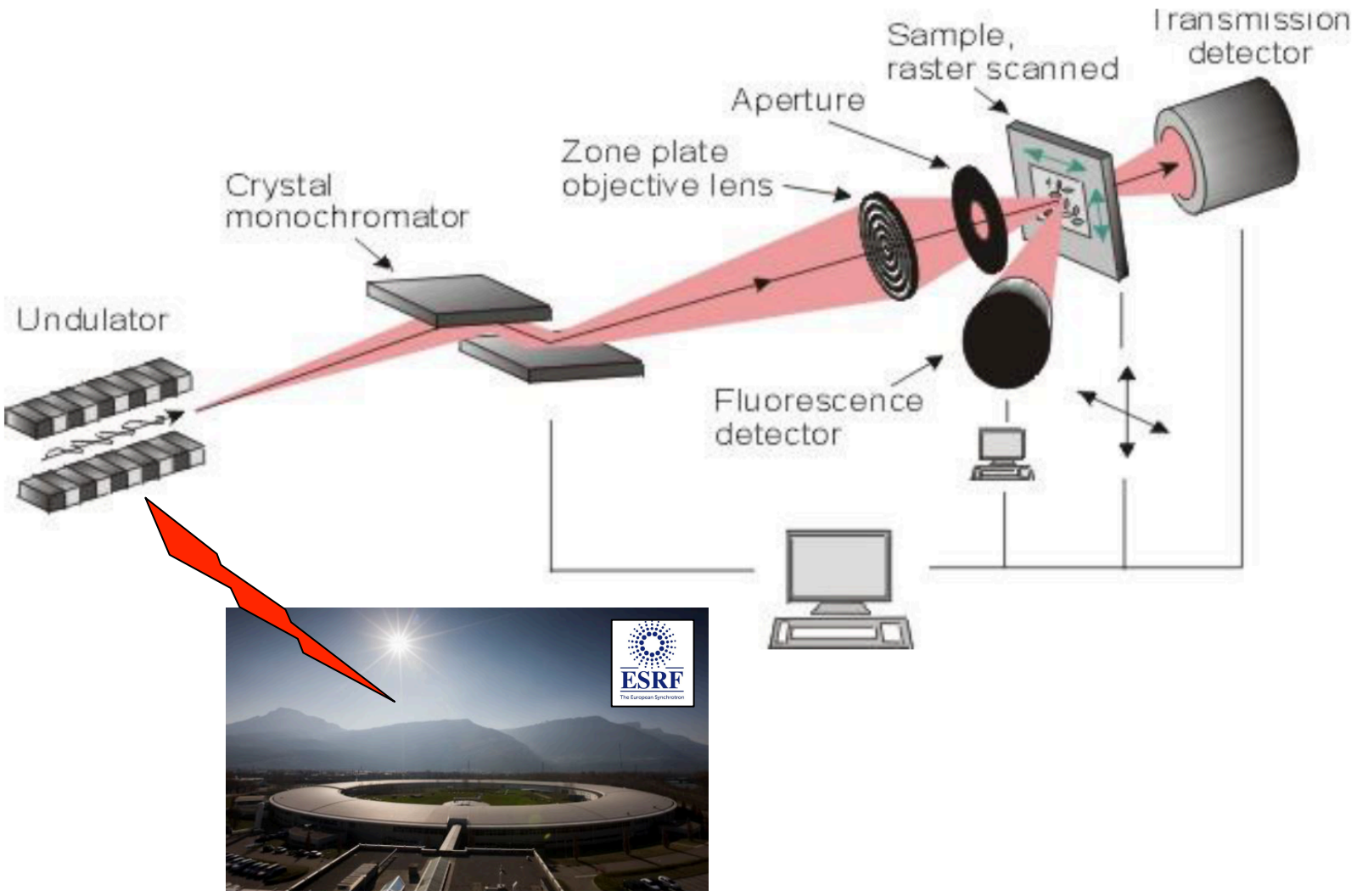

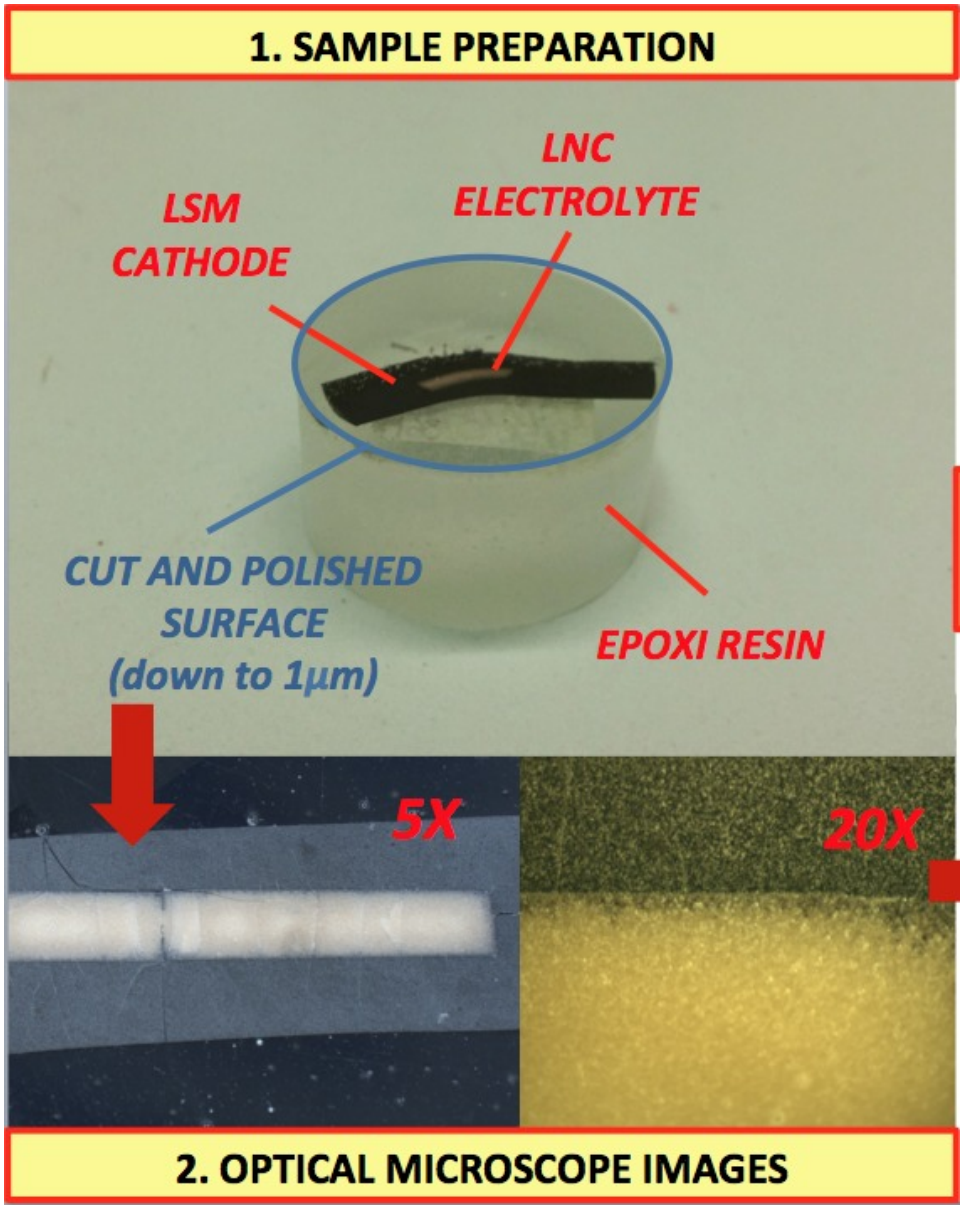

F. Giannici et al. Chem. Mater. 2015, 27, 2763

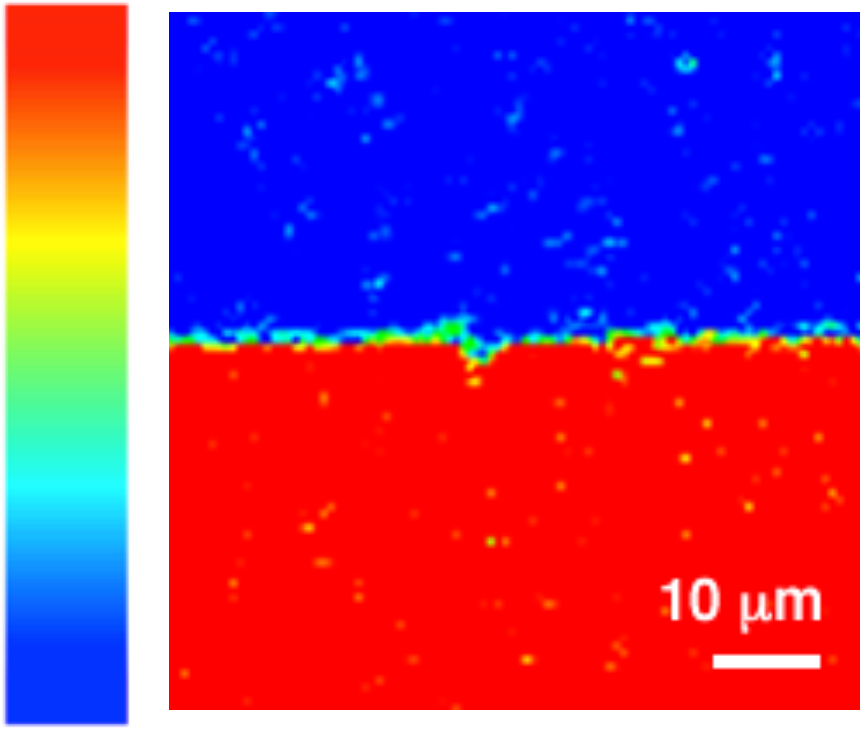

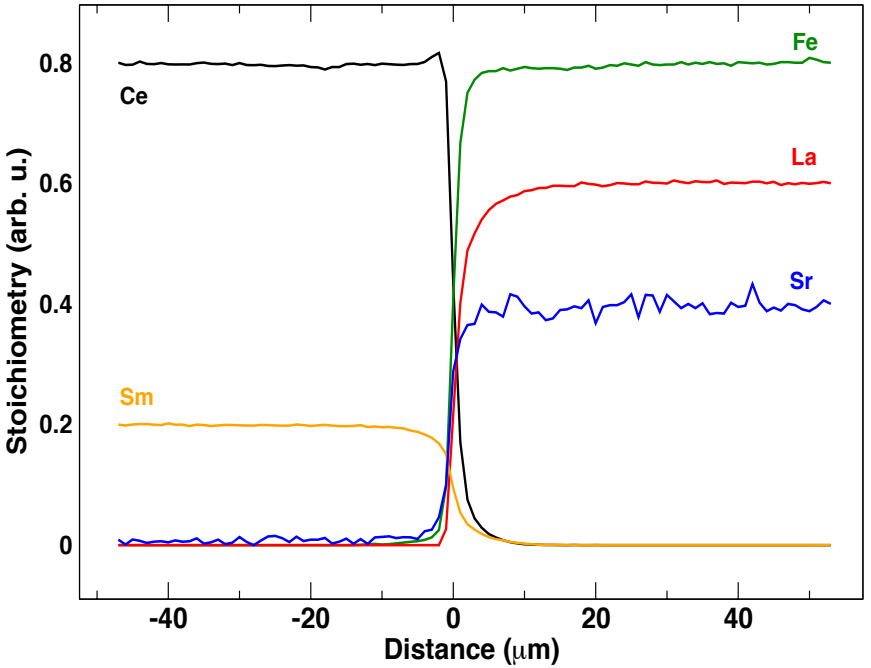

LSCF-SDC_12h at the Fe K-edge. Left: heatmap of the total fluorescence intensity; right: concentration profiles of cerium (black), lanthanum (red), strontium (blue), samarium (orange) and iron (green)

Sm depletion begins @2 μm before interface

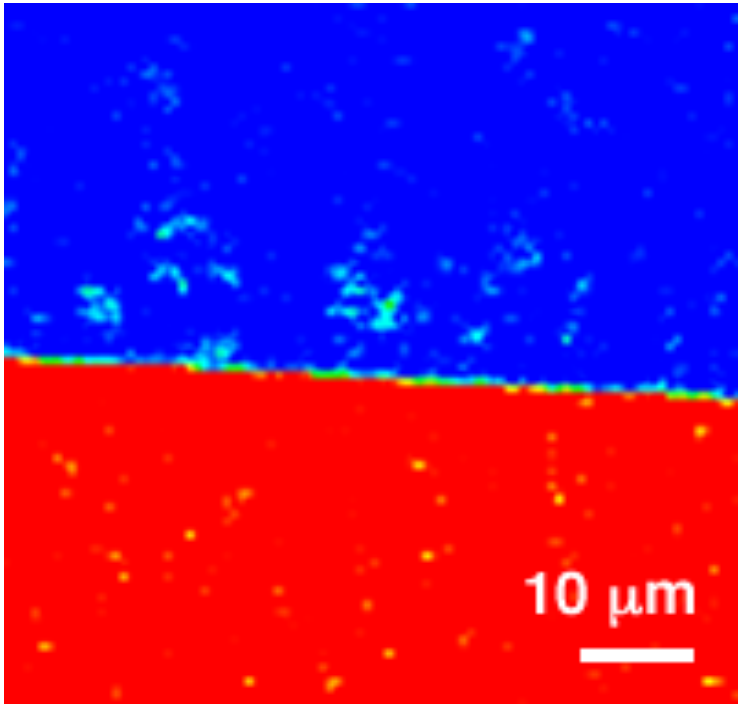

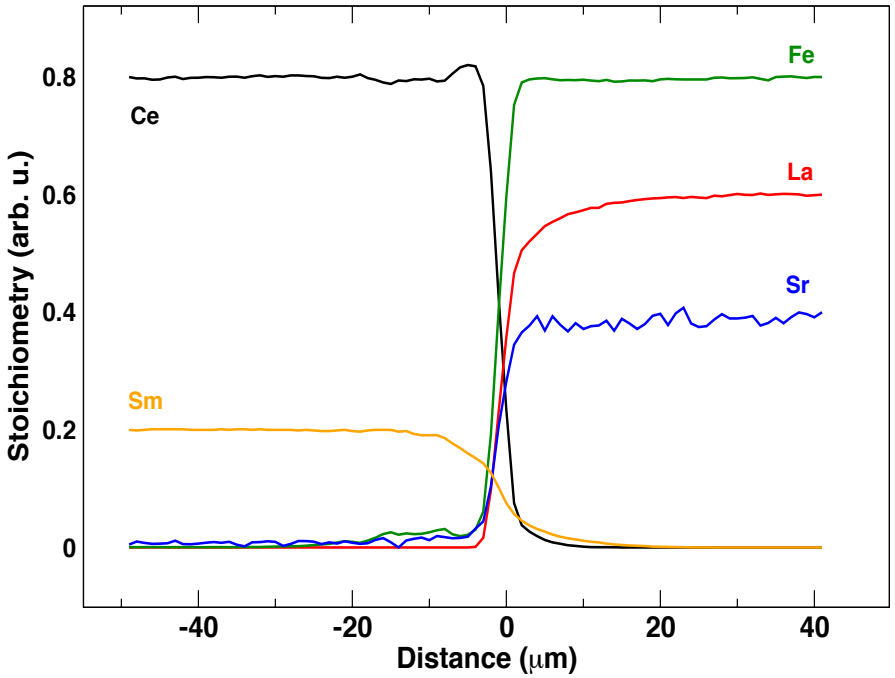

LSCF-SDC_72h at the Fe K-edge. Left: heatmap of the total fluorescence intensity; right: concentration profiles of cerium (black), lanthanum (red), strontium (blue), samarium (orange) and iron (green)

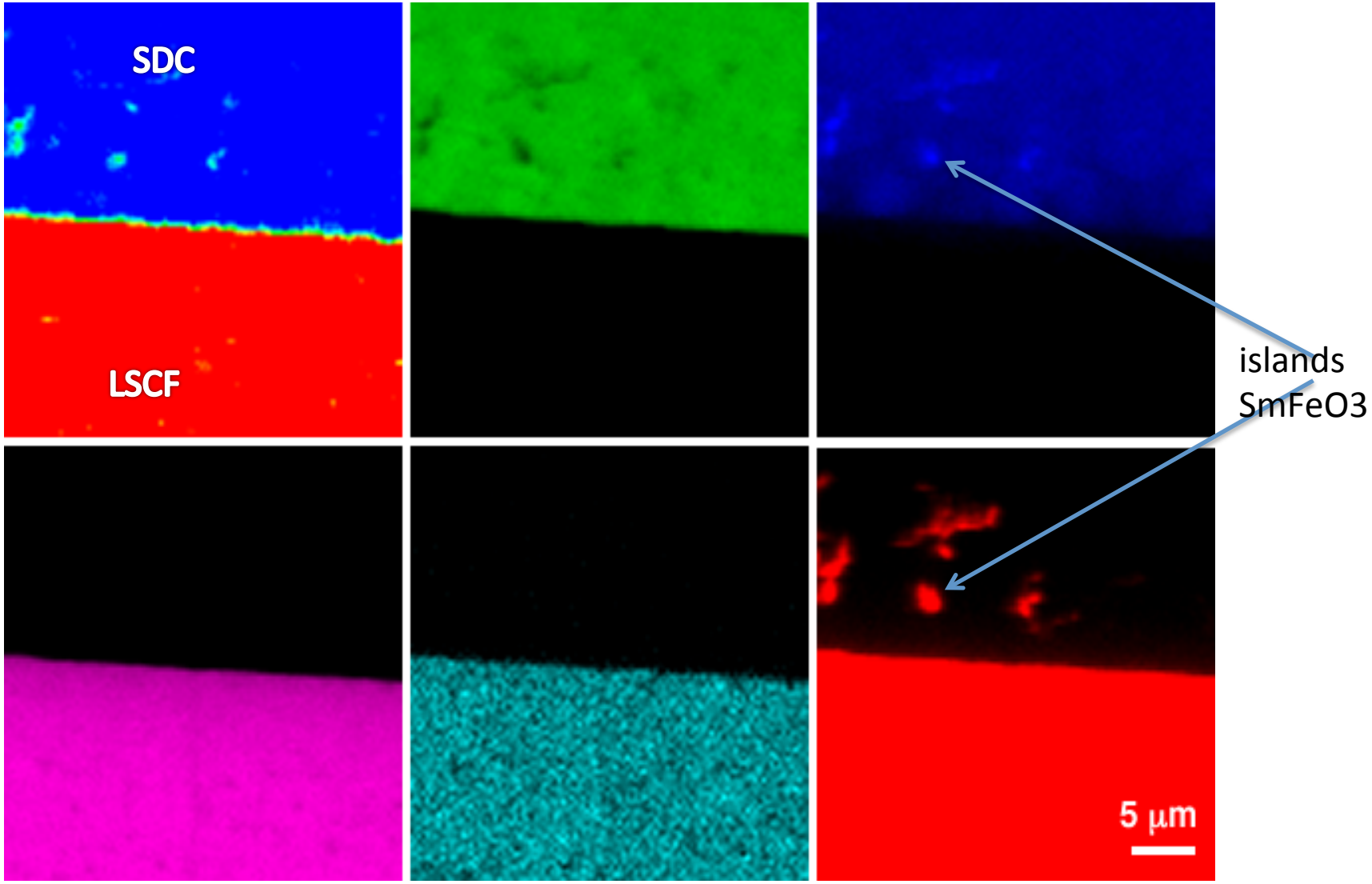

LSCF-SDC_72h at the Fe K-edge. Clockwise from top left:
heatmap of the total fluorescence intensity and concentration maps of cerium (green), samarium (blue), iron (red), strontium (cyan) and lanthanum (pink)

F. Giannici et al., under review

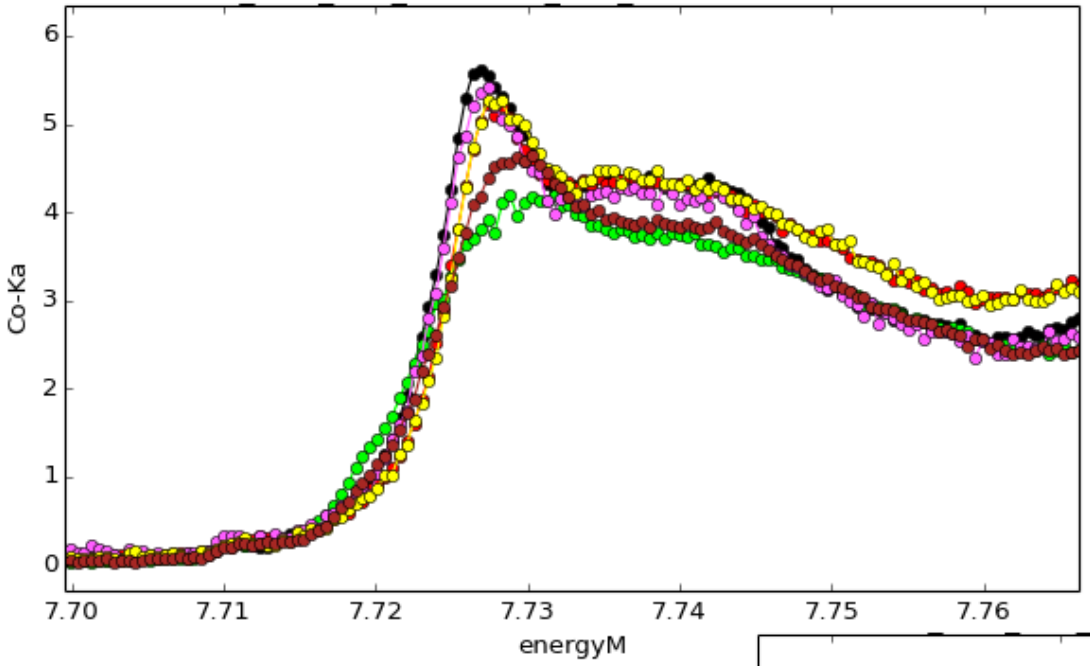

Co K-edge microXANES

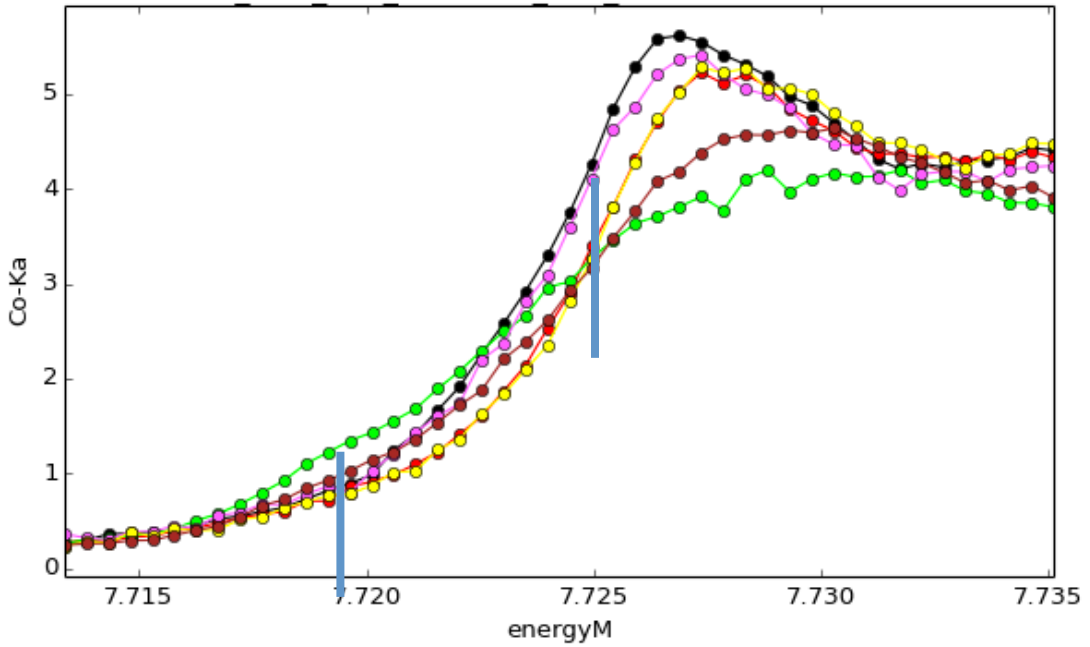

$La_{0.6}Sr_{0.4}Co_{0.2}Fe_{0.8}O_3$ / $Ce_{0.8}Sm_{0.2}O_2$

Mappe di speciazione chimica

$La_{0.6}Sr_{0.4}Co_{0.2}Fe_{0.8}O_3$

$Ce_{0.8}Sm_{0.2}O_2$

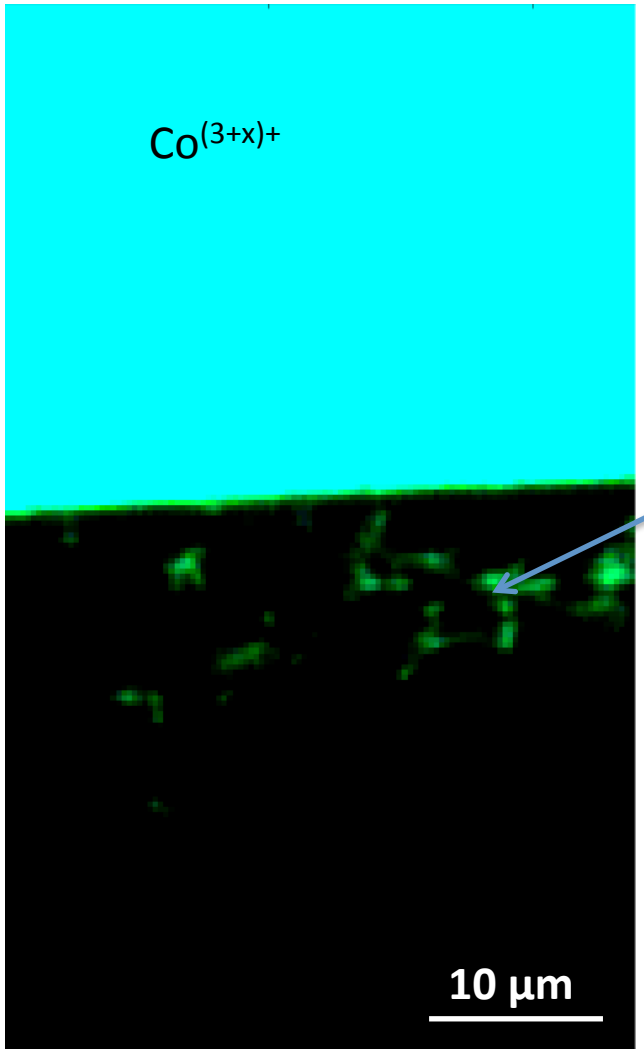

E = 7719 eV

E = 7725 eV

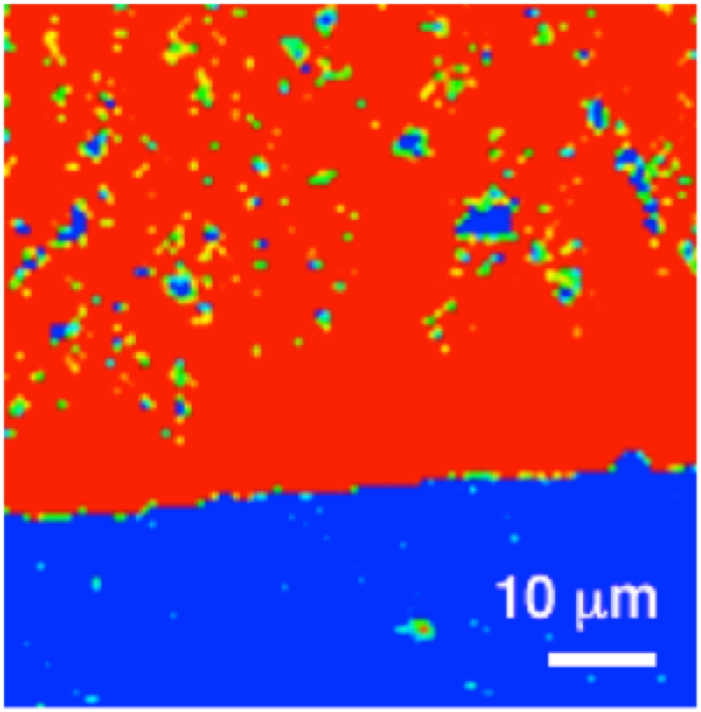

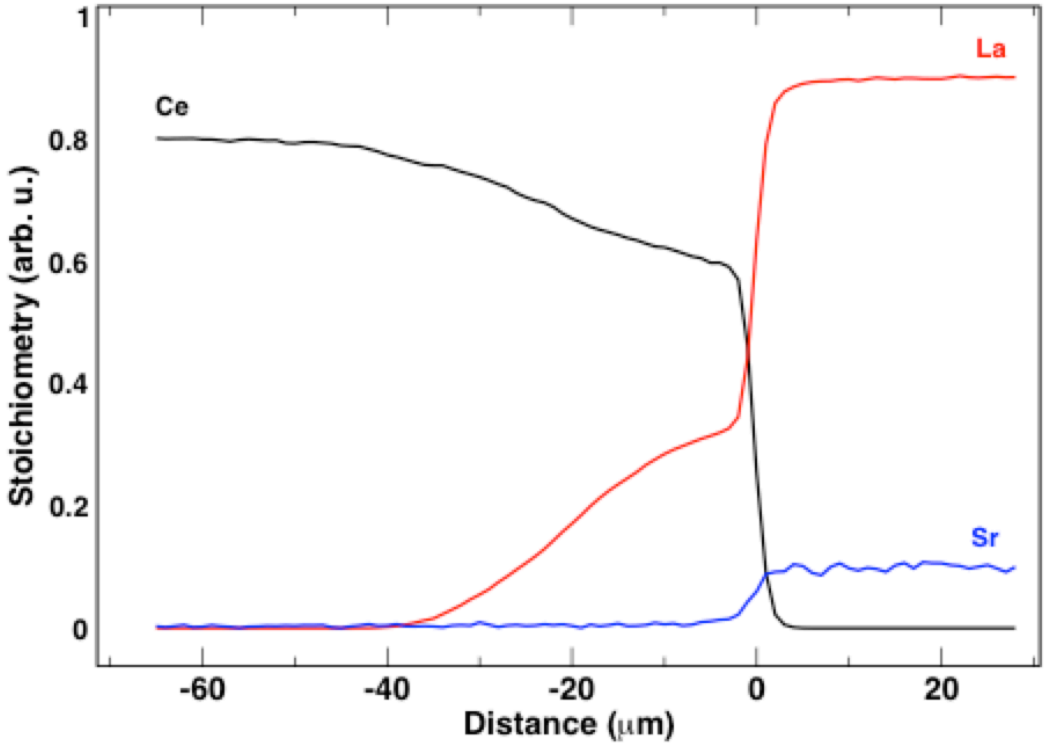

LSFCu-SDC_72h at the Ce L_3-edge. Left: heatmap of the total fluorescence intensity; right: concentration profiles of cerium (black), lanthanum (red) and strontium (blue)

the specular behaviour of Ce and La are particularly evident in this map taken at the Ce L3 edge

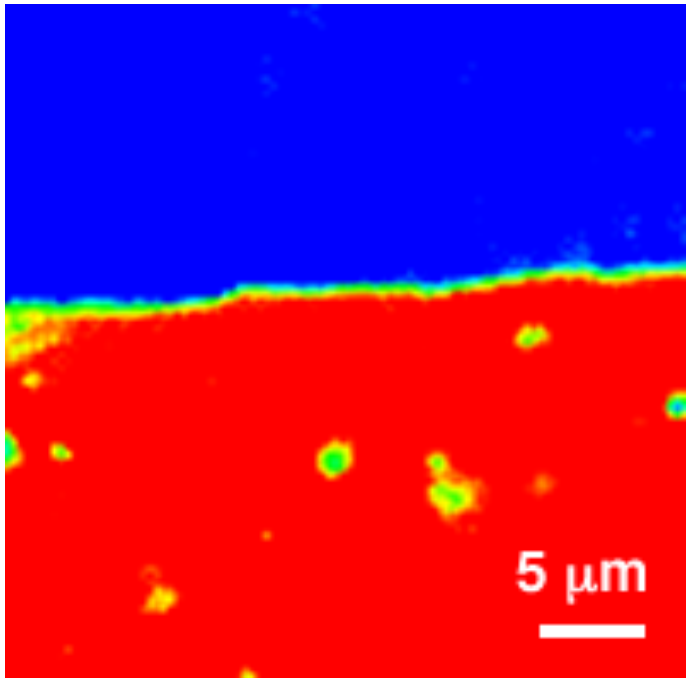

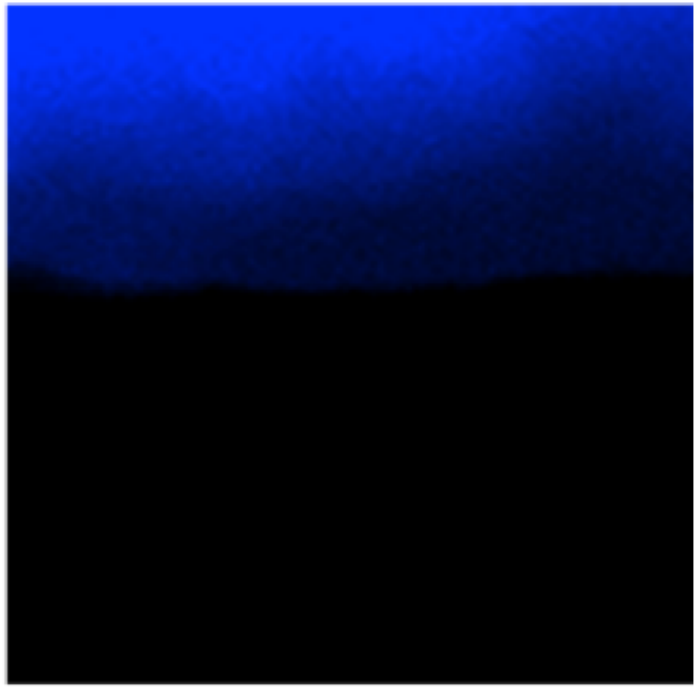

LSFCu-SDC_72h at the Fe K-edge. Left: heatmap of the total fluorescence intensity; right: concentration profiles of cerium (black), lanthanum (red), strontium (blue), samarium (orange) and iron (green)

diffusion of La
and corresponding depletion of Sm and Ce

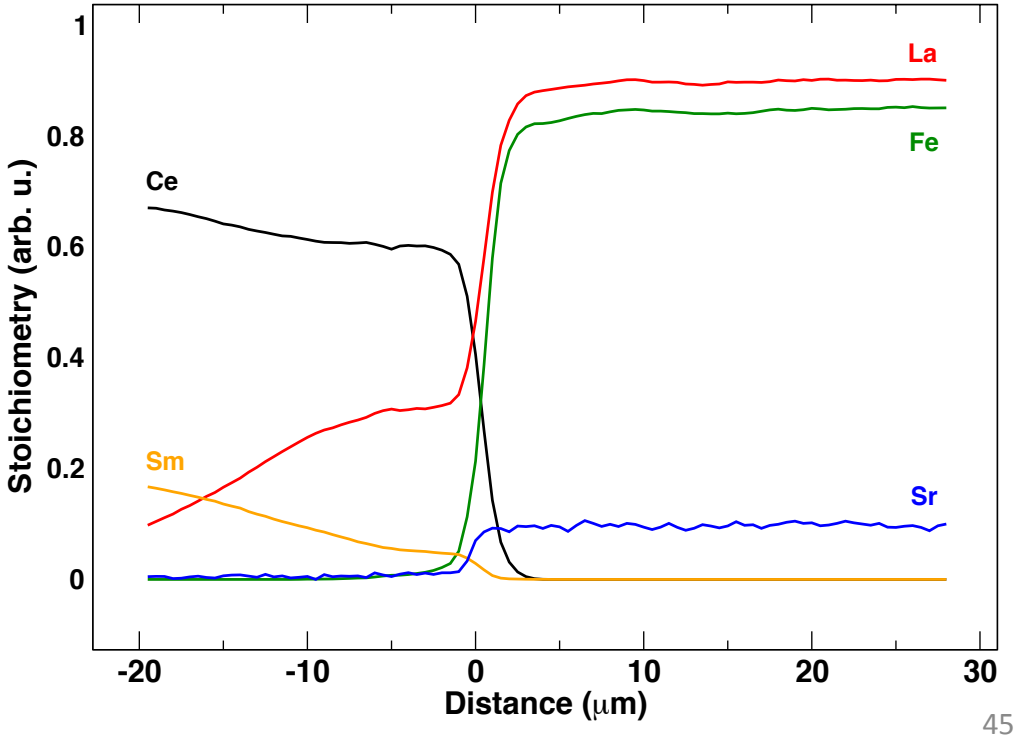

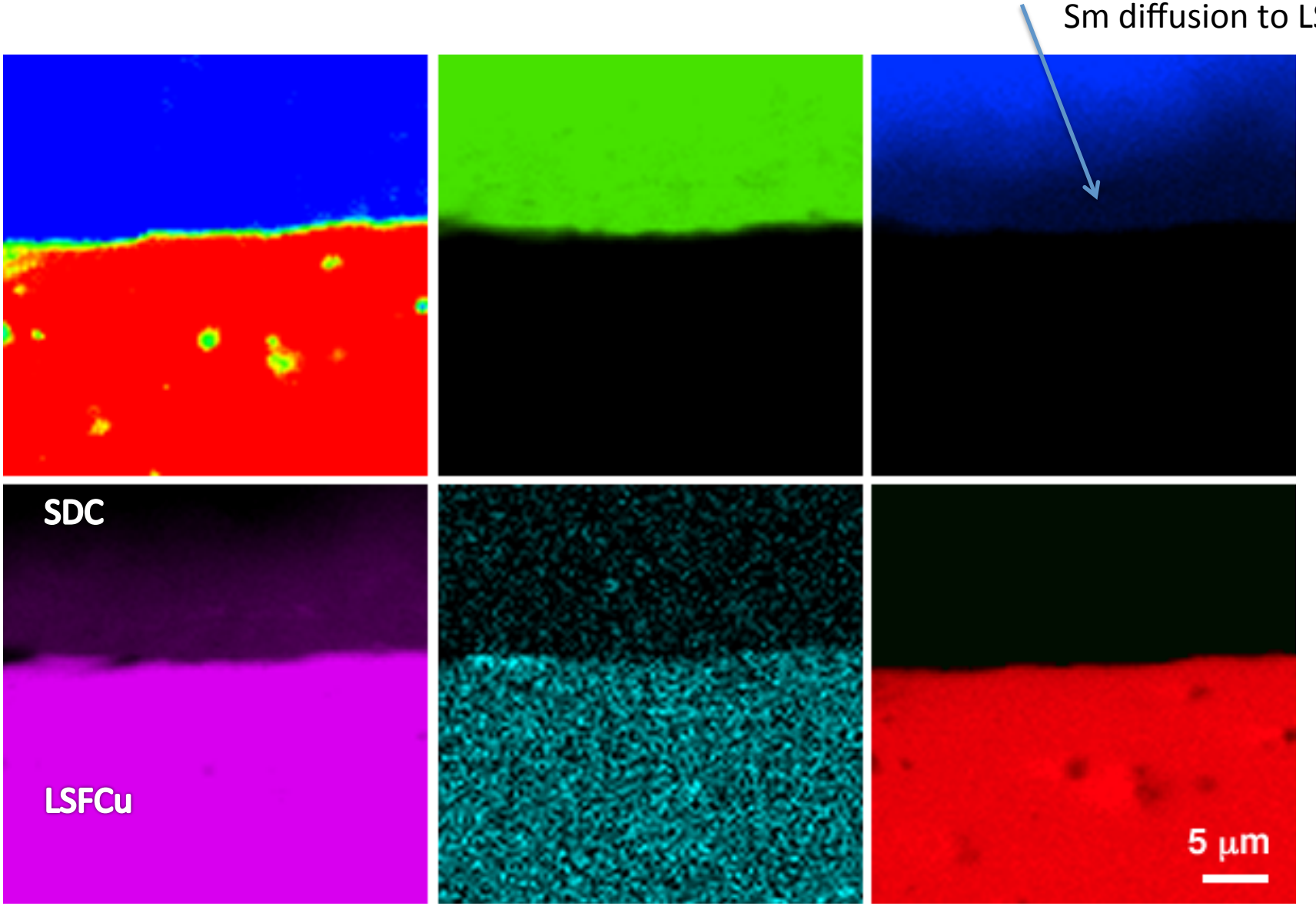

LSFCu-SDC_72h at the Fe K-edge. Clockwise from top left: heatmap of the total fluorescence intensity and concentration maps of cerium (green), samarium (blue), iron (red), strontium (cyan) and lanthanum (pink)

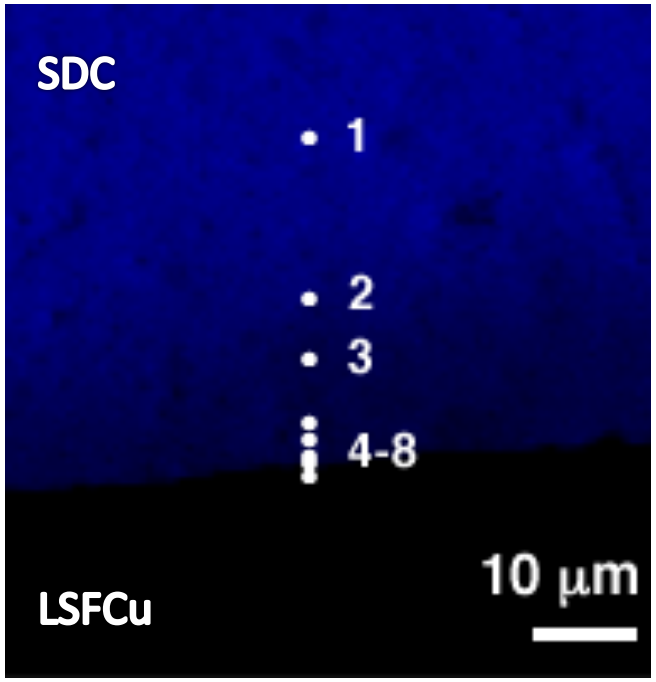

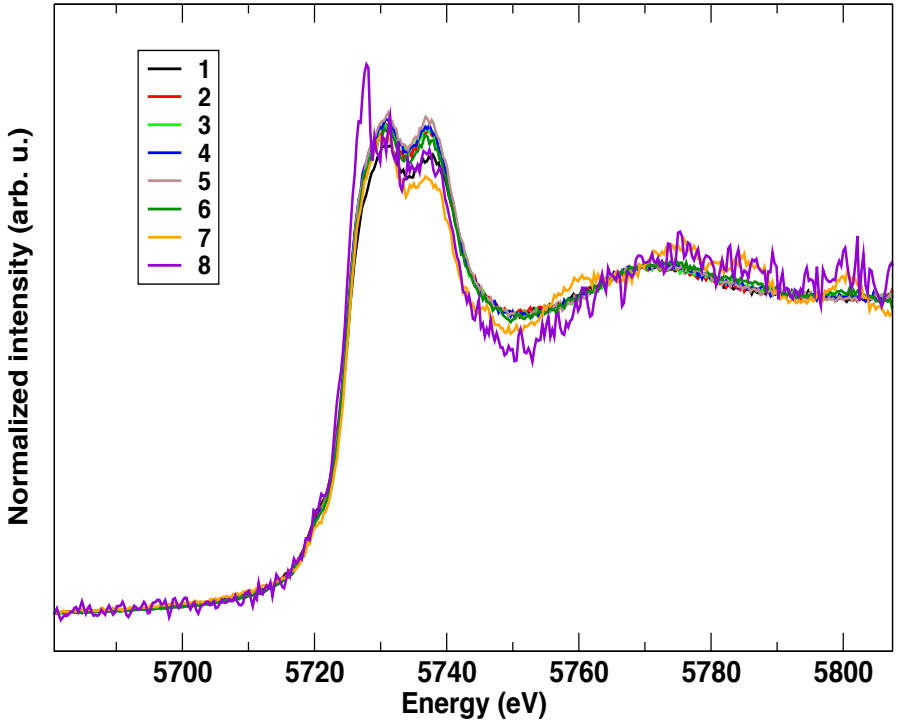

LSFCu-SDC_72h at the Ce L_3-edge. Left: concentration map of cerium (blue);
right: Ce L_3-edge microXANES spectra measured at different points shown in the left panel

Ce 4+: double peak at 5730 and 5737; Ce 3+: single peak at 5726
Ce diffuse and substitute La in LSFCu

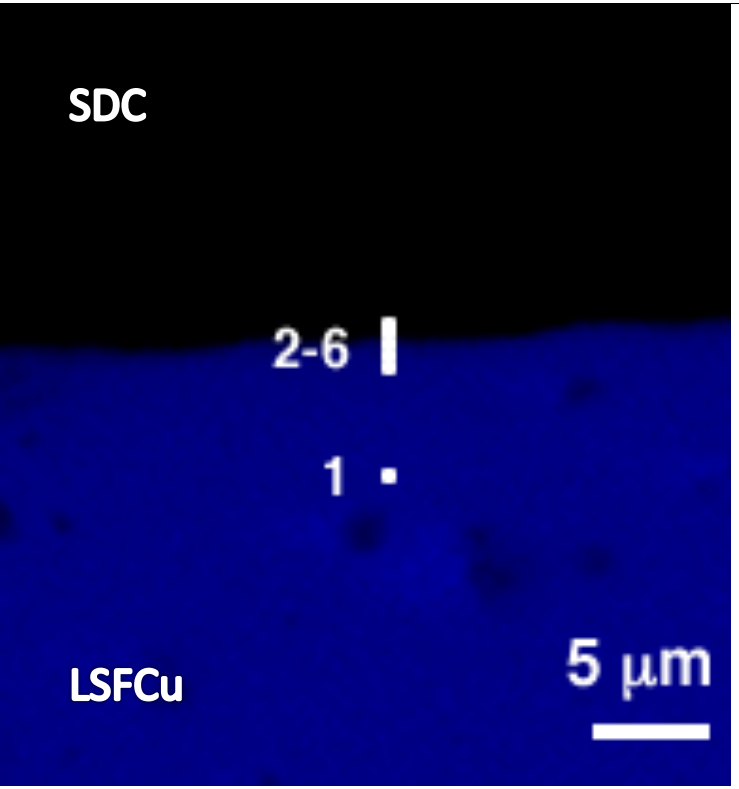

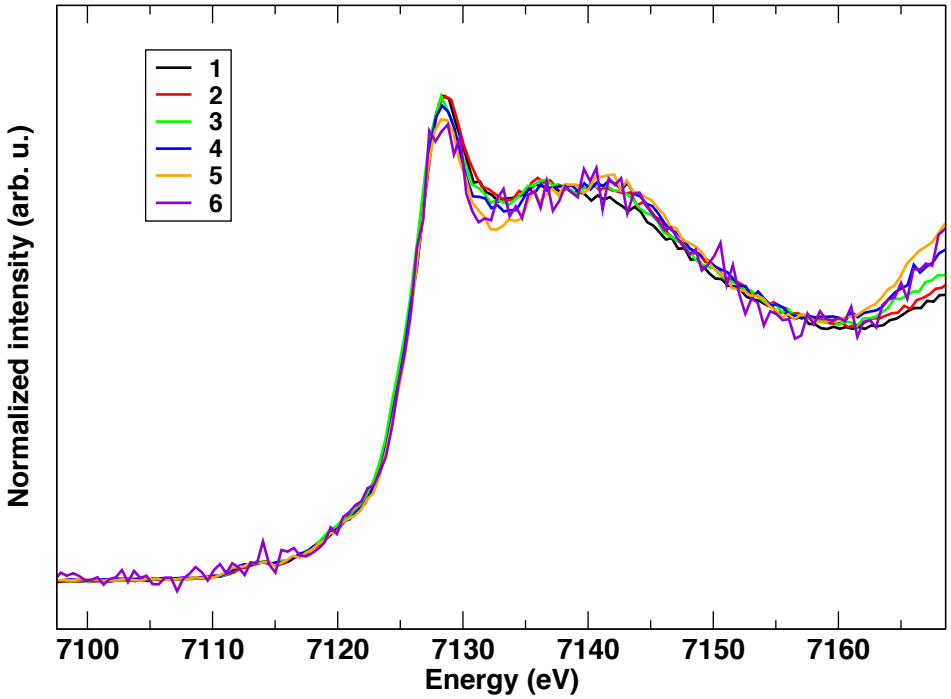

LSFCu-SDC_72h at the Fe K-edge. Left: concentration map of iron (blue); right: Fe K-edge microXANES spectra measured at different points shown in the left panel

iron does not change chemical state and coordination environment

Case studies

- batteries
- CO_2 capture by Chemical-Looping Combustion (CLC)
- electrode-electrolyte interdiffusion processes
- ***operando*** **investigation of Fuel Cell**

Escamicroscopy - SPEM layout

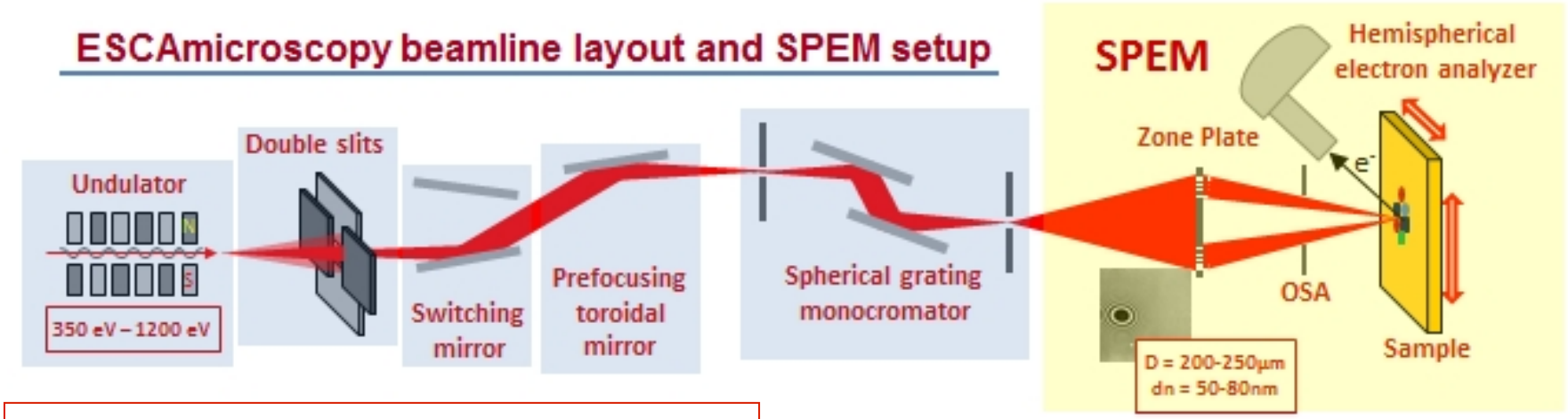

Milestones

- 1995:first user
- 2000-2004: new micros/prep chambers

- Linearly Polarised Undulator
- Photon energy range: 350 – 1200 eV
- SGM monochromator equipped with 2 gratings for low and high photon energy

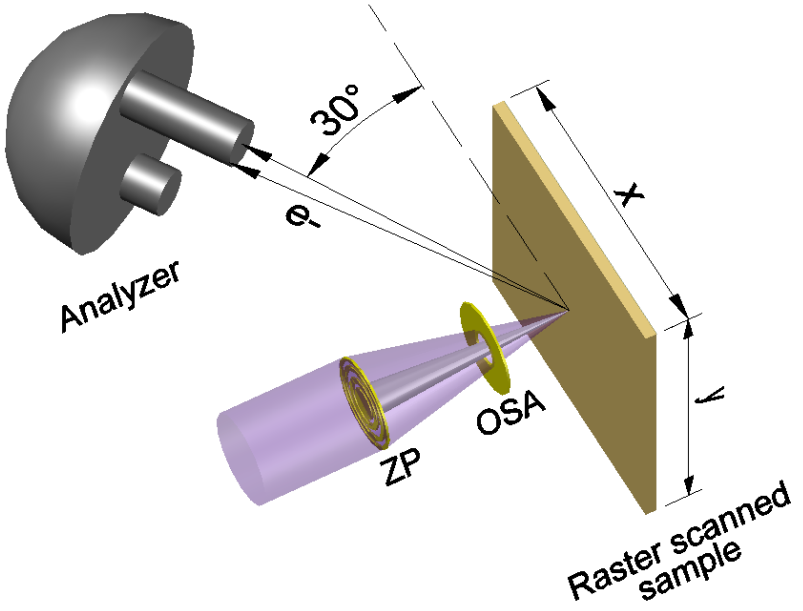

Top Catal (2016) 59:448–468
DOI 10.1007/s11244-015-0519-1

ORIGINAL PAPER

Recent Approaches for Bridging the Pressure Gap in Photoelectron Microspectroscopy

Andrei Kolmakov[1] · Luca Gregoratti[2] · Maya Kiskinova[2] · Sebastian Günther[3]

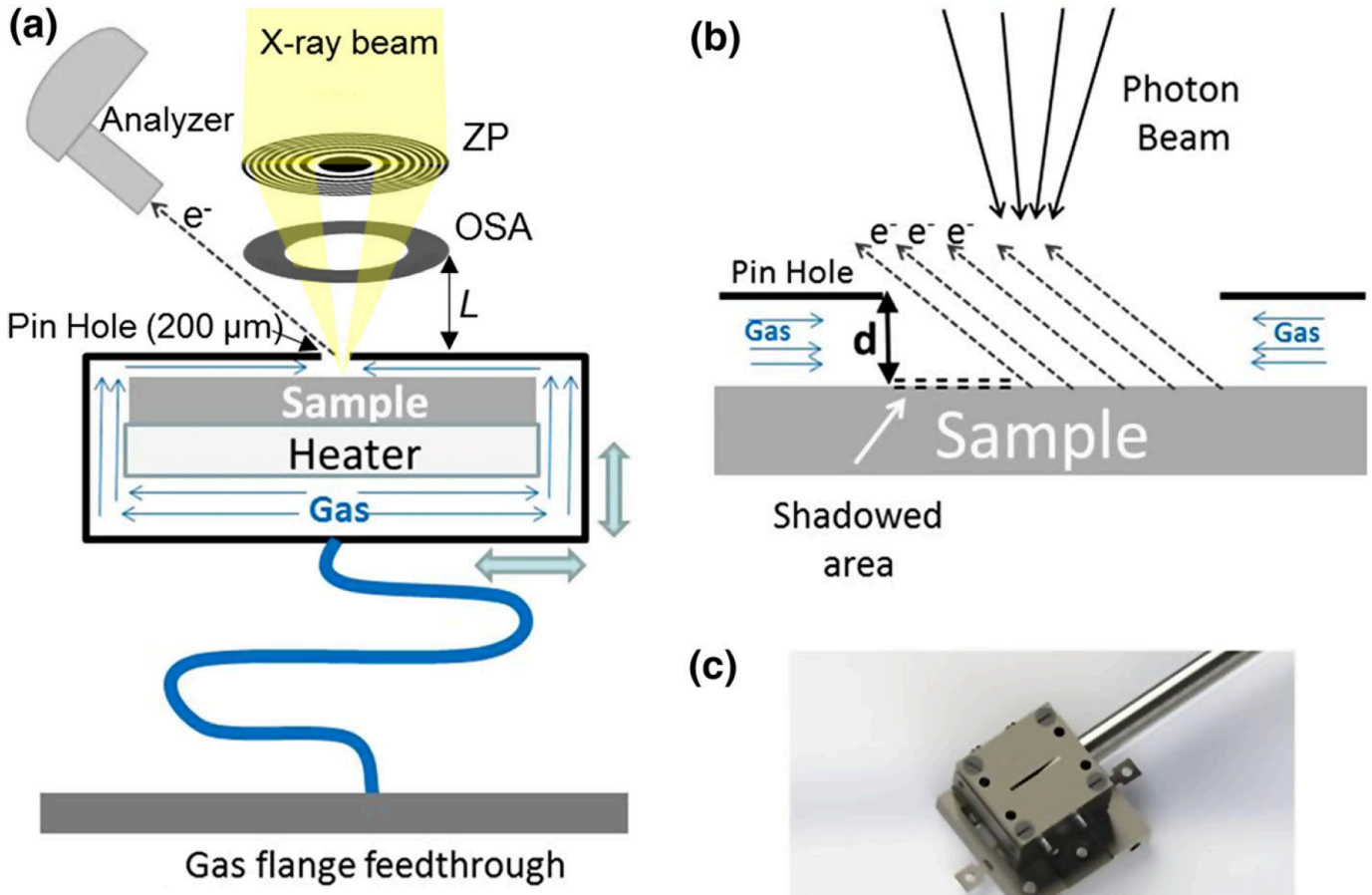

In-situ Photoelectron Microspectroscopy and Imaging of Electrochemical Processes at the Electrodes of a Self-driven Cell

Benedetto Bozzini[1], Matteo Amati[2], Luca Gregoratti[2] & Maya Kiskinova[2]

www.nature.com/scientificreports

SCIENTIFIC REPORTS | 3 : 2848 | DOI: 10.1038/srep02848

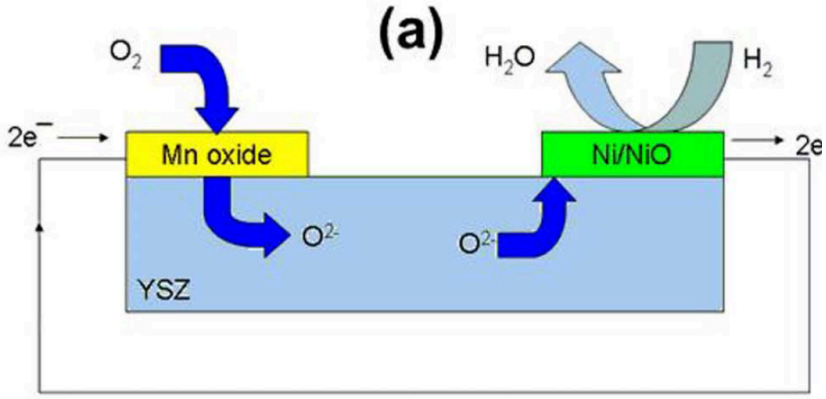

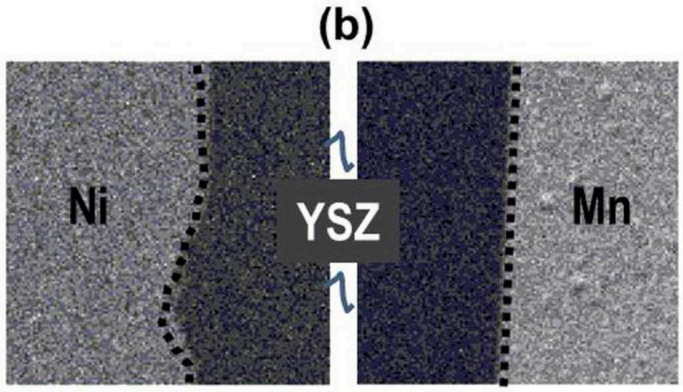

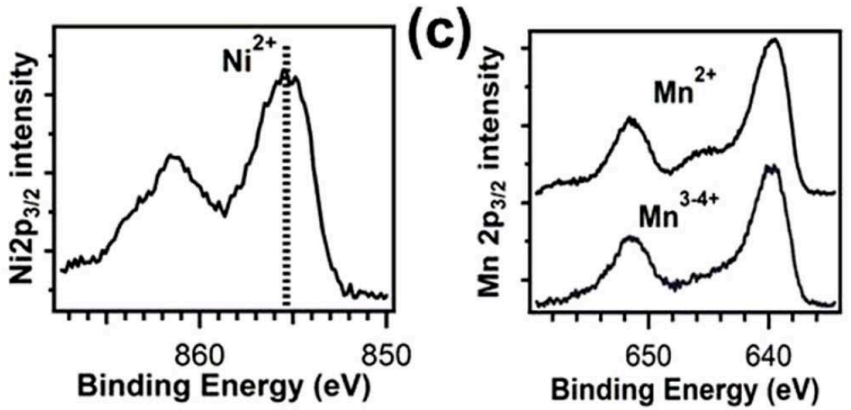

Figure 1 | (a) Scheme of the planar cell for in-situ electrochemical SPEM measurements. (b) Ni $2p_{2/3}$ and Mn 2p SPEM images (128 × 128 μm²) of the pristine cell (650°C): bright areas with sharp edges correspond to the Ni and Mn electrodes and the dark ones to the YSZ electrolyte. The dark dots close to the electrode edge indicate the most active region (c) Ni $2p_{2/3}$ and Mn 2p (bottom spectrum in Mn panel) μ-PES of the cell electrodes before starting the reaction (650°C). The top spectrum in the Mn panel corresponds to the partially reduced Mn state.

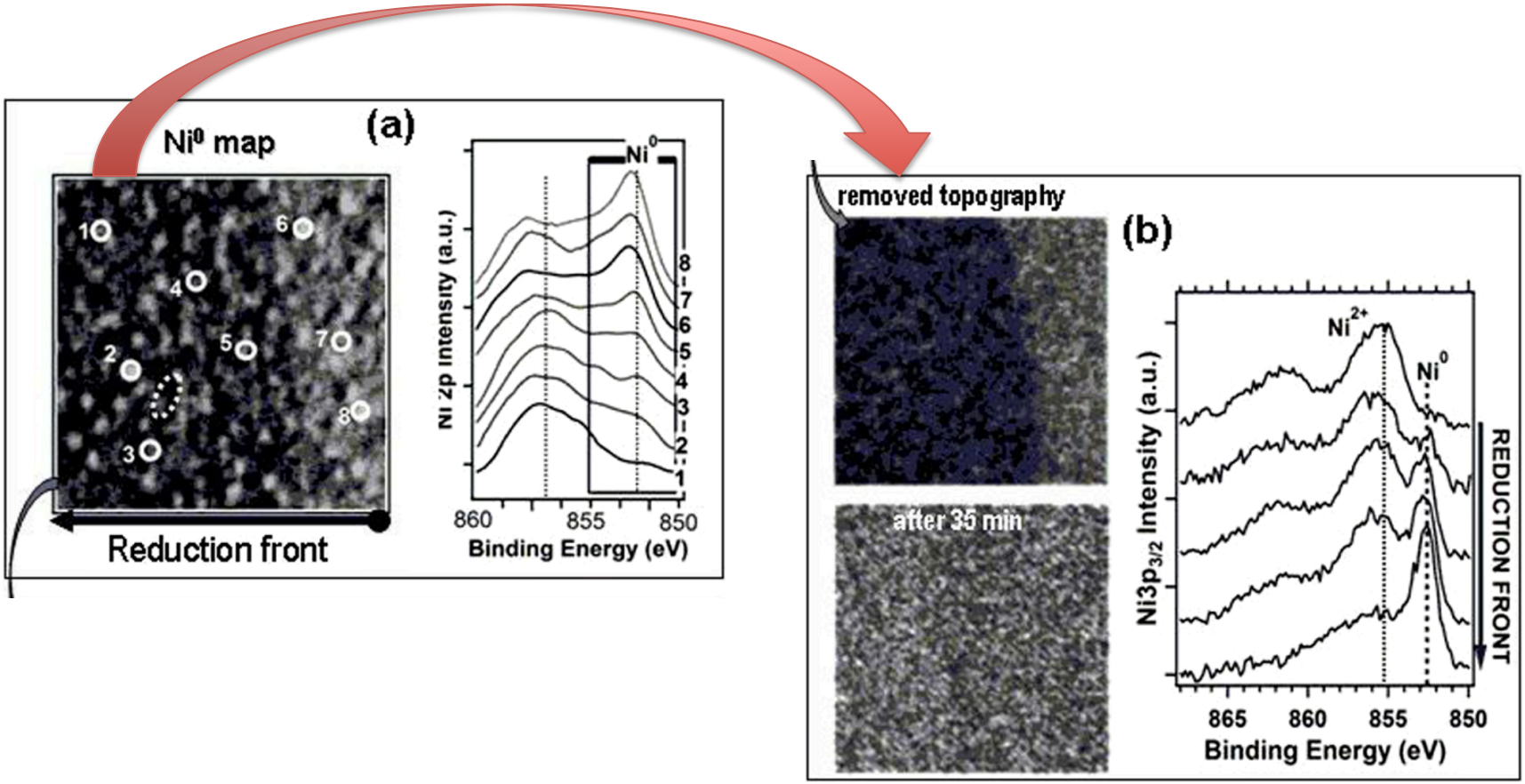

Figure 3 | (a) 32 × 32 μm² Ni^0 map (left) and Ni 2p spectra (right) taken in indicated locations immediately after switching from O_2 10^{-5} mbar to H_2 1 mbar (650°C). (b) Chemical maps obtained after removing the topography contrast from (a) (top) and taken after 35 minutes (bottom) (650°C). The topography contrast was removed by dividing the Ni^0 image to the background image[13]. The μ-PES spectra shown in the right panel were measured at regular time intervals in a micro-spot within the region indicated by the ellipse in Ni^0 map in (a). The dashed lines in the spectra panels indicate the position of the Ni 2p components and potential-induced shifts.